University of Crete
Department of Physics

Master's Thesis

Non-Hermitian Disordered Photonic Systems

Author:
Tzortzakakis Andreas

Supervisors:
Prof. E. N. Economou
Prof. K. G. Makris

A thesis submitted in partial fulfillment of the requirements for the degree of Master of Science

Heraklion, December 2020

Abstract

This master's thesis' subject is to provide a systematic theoretical study on the properties of photonic systems characterized by non-Hermitian disorder. Disordered systems have been extensively studied for decades, both due to their fundamental importance in Physics and their direct relevance to numerous technological applications. On the other hand, non-Hermiticity is a property of "open" systems - that is, of those that allow the exchange of energy with their environment - which has been recently revisited in optical physics in a totally different context, that of parity-time symmetry. The aforementioned twist led to the discovery of a plethora of new and exotic phenomena, which in turn led to the development of a whole new research field: that of non-Hermitian Photonics. In this work, we focus on the interplay between non-Hermiticity and disorder, along with the new properties that arise from the combination of these two features. At first, we study the phenomenon of Anderson localization in systems with uniform non-Hermitian disorder, by calculating the localization length and the spatial extent of the system's eigenstates, as well as the density of states and eigenvalue statistics on the complex plane. Next, we examine the properties of systems with non-Hermitian binary disorder. Emphasis is placed on the physical-behavior differences that they exhibit concerning their Hermitian analogs. Interestingly, several unexpected and intriguing effects make their appearance in our model. The relation of our findings to recent experimental results is also discussed. Finally, we present a method for achieving perfect and shape-preserving beam transmission through discrete photonic environments characterized by disorder. This is achieved by carefully combining the effects of disorder and non-Hermiticity, in such a way that one phenomenon negates the influence of the other. Remarkably, the effects of both diagonal and off-diagonal disorder can be efficiently eliminated by our non-Hermitian design.

Περίληψη

Η μεταπτυχιακή αυτή εργασία αποτελεί μία συστηματική μελέτη των ιδιοτήτων φωτονικών συστημάτων που χαρακτηρίζονται από μη-Ερμητιανή αταξία (non-Hermitian disorder). Η αταξία είναι μία φυσική ιδιότητα που έχει αποτελέσει αντικείμενο έντονης ερευνητικής δραστηριότητας για δεκαετίες, τόσο λόγω του θεμελιώδους ρόλου που παίζει στη Φυσική, όσο και λόγω της άμεσης συσχέτισης της με συστήματα τεχνολογικού ενδιαφέροντος. Από την άλλη, η μη-Ερμητιανότητα είναι μια ιδιότητα των «ανοιχτών» συστημάτων (αυτών δηλαδή που επιτρέπουν την ανταλλαγή ενέργειας με το περιβάλλον τους), η οποία επανεξετάστηκε πρόσφατα στο πεδίο της οπτικής Φυσικής σε ένα εντελώς διαφορετικό πλαίσιο, αυτό της χωροχρονικής συμμετρίας ($\mathcal{PT}$ symmetry). Η ιδέα αυτή οδήγησε στην ανακάλυψη πληθώρας νέων και εξωτικών φυσικών φαινομένων και, εν συνεχεία, στη δημιουργία ενός ολόκληρου ερευνητικού κλάδου: αυτού της μη-Ερμητιανής Φωτονικής (non-Hermitian Photonics). Σε αυτή την εργασία επικεντρωνόμαστε στην αλληλεπίδραση μεταξύ μη-Ερμητιανότητας και αταξίας, καθώς και στις νέες ιδιότητες που προκύπτουν από τον συνδυασμό των δύο αυτών φαινομένων. Αρχικά μελετάμε τον εντοπισμό Άντερσον (Anderson localization) σε πλέγματα από φωτονικά στοιχεία, υπολογίζοντας το μήκος εντοπισμού (localization length) και την χωρική έκταση των ιδιοκαταστάσεων του συστήματος, καθώς και τη στατιστική των ιδιοτιμών του στο μιγαδικό επίπεδο. Στη συνέχεια, εξετάζουμε πλέγματα μη-Ερμητιανής δυαδικής αταξίας (binary disorder) και τις διαφορές στη φυσική συμπεριφορά που παρουσιάζουν σε σχέση με τα Ερμητιανά τους ανάλογα, βρίσκοντας ότι διάφορα απρόσμενα και ενδιαφέροντα νέα χαρακτηριστικά κάνουν την εμφάνισή τους. Σχολιάζεται επίσης η συσχέτιση μεταξύ των αποτελεσμάτων μας και πρόσφατων πειραματικών ευρημάτων. Τέλος, παρουσιάζουμε μια μέθοδο για την επίτευξη τέλειας διέλευσης διαμέσου άτακτων συστημάτων, συνδυάζοντας τις νέες δυνατότητες που προκύπτουν από το συνδυασμό των δύο φαινομένων που εξετάζουμε με τέτοιο τρόπο, ούτως ώστε το ένα φαινόμενο να αναιρεί την επίδραση του άλλου και το σύστημα να συμπεριφέρεται σαν να χαρακτηρίζεται από πλήρη τάξη.

Acknowledgments

First and foremost, I would like to express my sincere gratitude to my supervisors, Prof. Eleftherios Economou and Prof. Konstantinos Makris, who guided me throughout this project.

In particular, I wish to express my deep appreciation to Prof. Economou for being an inspiring teacher and an example scientist for me. Our discussions through all these years helped me obtain a deeper and interdisciplinary knowledge of Physics.

I would also like to acknowledge Prof. Makris for introducing me to the world of scientific research and empowering my skills measurably in the area of classical Optics. Without his continuous support and guidance, this work would have never been completed.

Moreover, I especially thank Prof. Stefan Rotter for his valuable advice and support. It's been an honor working with him.

I am also grateful to my friend and colleague Evangelos Tsolakidis for valuable discussions and assistance at every stage of this project.

Finally, I wish to extend my special thanks to my friends and family who supported me and offered deep insight into the study.

Thesis Output

Publications

- A. F. Tzortzakakis, K. G. Makris and E. N. Economou, Phys. Rev. B **101**, 014202 (2020). (link)
- A. F. Tzortzakakis, K. G. Makris, S.Rotter and E. N. Economou, Phys. Rev. A **102**, 033504 (2020). (link)
- A. F. Tzortzakakis, K. G. Makris, A. Szameit and E. N. Economou, Under peer review - arXiv:2007.08825 (2020). (link)

Conference Proceedings

- A. F. Tzortzakakis, K. G. Makris, S. Rotter and E. N. Economou. FiO+LS (pp. FM2C-2), OSA (2020). (link)
- A. F. Tzortzakakis, K. G. Makris, A. Szameit and E. N. Economou. FiO+LS (pp. FTh5B-5), OSA (2020). (link)

List of Symbols

The next list describes several symbols that will be later used within the body of the document

ψ_n	Complex electric-field amplitude at the n^{th} waveguide channel (site).
ϵ_n	Site element/propagation constant of the n^{th} waveguide channel.
z	Normalized propagation distance along the waveguide axis.
$c_{n,m}$	Coupling coefficient between the (nearest neighboring) channels n and m. In most cases, $c_{n,m} = \text{const.} \equiv c$, and we set $c = 1$ for simplicity.
ω	System's eigenvalue (complex in general).
W	Disorder strength, in the case of uniform distribution of disorder (any random variable $\in [-\frac{W}{2}, \frac{W}{2}]$).
DOS	Density of states.
ξ	Localization length, defined by Eq. 2.16.
N	Total number of sites (for 1-D lattices).
$\mathrm{P}(s)$	Probability distribution P of normalized nearest-neighbor energy spacings s (see Eq. 3.6).
$\hat{\mathrm{H}}$	The Anderson model Hamiltonian (see Eqs. 2.3, 3.3).
T, R	Transmittance and reflectance, respectively.
k	Wavenumber.
$\mathcal{P}(z)$	Electric field power as a function of the propagation distance z.

Table of Contents

Chapter 1

Introduction

The study of crystalline solids is based on Bloch's theorem [1, 2] which assumes a perfect periodicity in the positions of the atoms and in the density of electrons. However, in actual crystalline solids there are always deviations from periodicity, such as point defects, linear faults (e.g. dislocations), 2D defects (e.g. interfaces of crystallites); if the concentration of these deviations becomes high enough Bloch's theorem breaks down and a new paradigm emerges featuring novel properties such as the possibility of localized eigenstates [3, 4]. The concept of this so-called Anderson localization, which claims that an electronic wave can be trapped in a finite region of a disordered lattice, has been at the center of the attention of the solid state physics community for more than sixty years [5, 6, 7, 8, 9, 10]. The localization phenomenon appears due to the interference among multiple scattering processes of the electronic waves by random variations in the potential of the crystal lattice. As a result of this interference, the previously extended eigenmodes of the system, the Bloch waves, may now become localized eigenstates which decay exponentially for large distances.

The phenomenon of Anderson localization has also been studied experimentally, indirectly, by measurements of macroscopic quantities such as the conductance [11, 12, 13, 14] and the transmission [15, 16, 17, 18]. In solid state systems though, the existence of many body interactions and temperature dependent effects, such as inelastic scattering, makes the interpretation of these experiments rather complex. In order to overcome this difficulty, the topic of localization was extended to the regime of optics, acoustics and elastics where its consequences were not clouded by other effects producing similar observations [19, 20, 21, 22, 23, 24, 25, 26]. Such an extension is naturally valid, since the concept of localization is based on wave scattering and interference [27, 28]. The only difficulty with classical waves, such as electromagnetic ones, is that they usually exhibit very weak scattering not enough

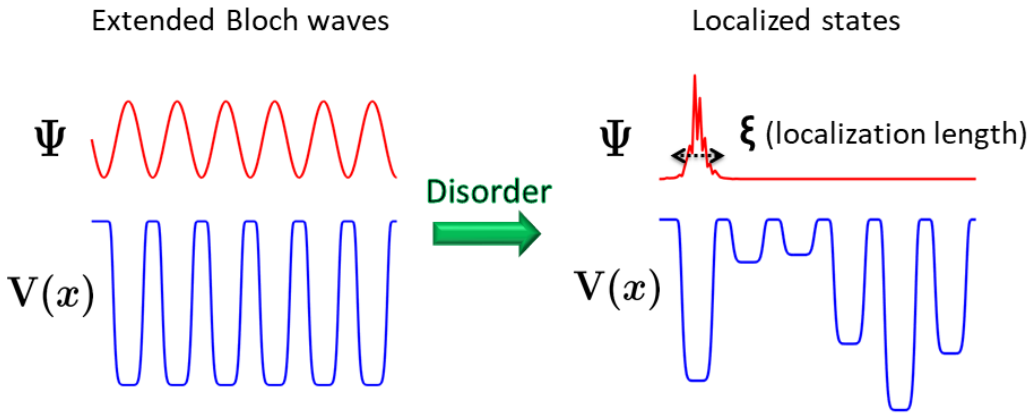

Figure 1.1: Schematic depiction of the Anderson localization phenomenon. Left column: amplitude of a Bloch wave (red line) propagating in a periodic potential (blue line). Right column: the introduction of disorder in the previous periodic potential (blue line) turns the extended Bloch wave to a spatially confined state of localization length ξ (red line).

to produce localization. Several ideas were proposed to circumvent this difficulty, some of which [29, 30] led through different paths to photonic crystals [31, 32, 33, 34, 35, 36] and phononic crystals [37, 38, 39, 40, 41, 42, 43].

Furthermore, another topic of intense research interest these days is wave propagation through complex disordered media, due to its immediate physical and technological relevance. As mentioned before, the presence of disorder leads to phenomena such as multiple scattering and Anderson localization. A direct manifestation of such wave scattering is the highly complex intensity pattern that is formed due to multi-path interference. With the advent of spatial light modulators and wavefront shaping techniques, interest has been growing in controlling such scattering pattern of waves propagating in complex media, for various novel applications in imaging and detection establishing the area of disordered Photonics [44, 45, 46, 47]. A great challenge is to overcome the detrimental effects of multiple scattering to achieve enhanced transmission through such a complex medium of disorder. A variety of experimental methods has been recently proposed [48, 49, 50, 51, 52, 53, 54]. However, most of these techniques rely on the existence of transmission resonances of the random medium and as a result require sophisticated wavefront shaping methods and adaptive imaging iteration algorithms. An alternative strategy would be to modify the scattering medium, instead of the incoming optical beam.

In an other direction, the study of optical structures characterized by

amplification (gain) and dissipation (loss) has led to the development of a new research field, that of non-Hermitian Photonics [55, 56, 57, 58, 59, 60, 61]. In particular, the introduction of the concepts of parity-time ($\mathcal{PT}$) symmetry [62, 63, 64] and exceptional points [65, 66, 67, 68, 69, 70] in optics, where gain and loss can be physically implemented [71, 72, 73, 74, 75, 76], triggered a number of theoretical and experimental works, which have demonstrated the potential applications of such non-Hermitian systems. The rich behavior and novel features of these structures has led to a plethora of experimental realizations of various optical devices spanning from unidirectional invisibility to broadband wireless power transfer [77, 78, 79, 80, 81, 82, 83, 84].

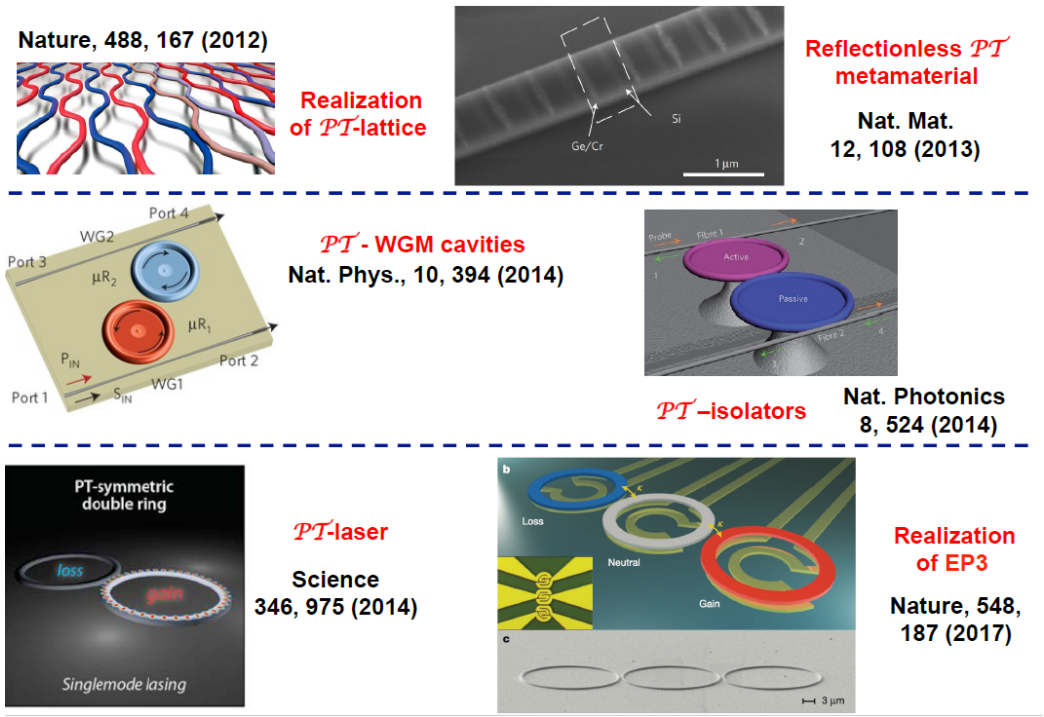

Figure 1.2: Some of the key experiments that were demonstrated recently in the context of non-Hermitian Photonics and $\mathcal{PT}$ symmetry.

In addition, non-Hermitian random matrices are a topic of intense research interest in the context of mathematical physics [85], and disordered Photonics [45, 86]. More specifically, random lasers [87, 88] where the decay of the cavity modes and the gain material leads naturally to dissipation and amplification, respectively, are a prototypical system in the framework of disordered complex media, where non-Hermiticity plays a crucial role.

In this thesis we will study systems that are characterized by non-Hermitian disorder and try to understand the physical behavior that results from the

combination of these two different effects. The realization of such systems is more appropriate for photonic rather than solid state systems, since the former can easily incorporate and realize complex potentials that require physical gain and loss. In our study we will make use of the methods developed within the context of Anderson localization in solid state physics as well as the techniques of electromagnetic wave scattering.

At first we will try to answer some of the main questions that stem from the interplay of disorder and non-Hermiticity in two-spatial dimensions, while comparing our results with the corresponding, well known characteristics of the Hermitian case. In particular, we will examine physically realistic Anderson type of non-Hermitian waveguide lattices, like the ones shown in Fig. 1.3, with the most general uncorrelated disorder that includes gain and/or loss. We are interested in studying the spectrum and the eigenvalue statistics of the model, as well as the extent length of its eigenvectors.

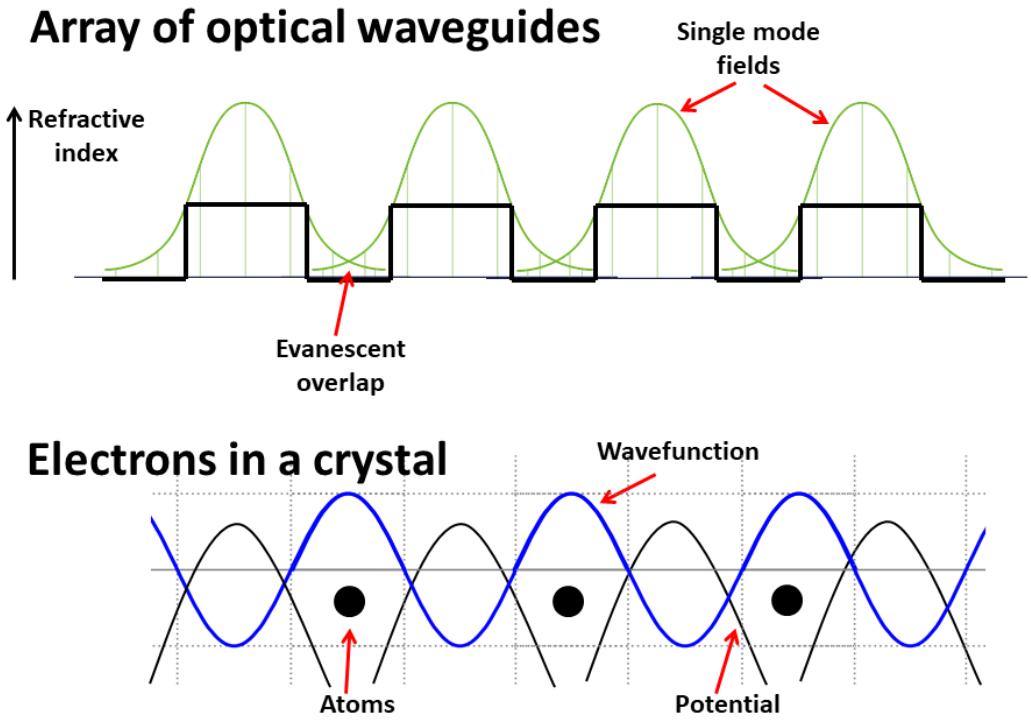

Figure 1.3: Schematic depiction of the equivalence between optical wave propagation in an array of coupled waveguide channels (upper part) and electronic propagation in a solid crystal (lower part). The array of coupled waveguides will be the main physical system of study in this work.

In what follows, we will study the effect of non-Hermiticity on a short-

range correlated 1-D disordered lattice which, in its Hermitian version, has been studied extensively for its unexpected delocalized states [89]. The diagonal matrix elements of our Hamiltonian take randomly two complex values ϵ and ϵ^*, each one assigned to a pair of neighboring sites. We will show that, contrary to the Hermitian case, all states in our system are localized. In addition, the obtained eigenvalue spectrum exhibits an unexpected intricate fractal-like structure on the complex plane. Moreover, with increasing non-Hermitian disorder, the eigenvalues tend to coalesce in particular small areas of the complex plane, a characteristic we term "eigenvalue condensation". Despite the Anderson localization of all eigenstates, the system exhibits an interesting dynamic behavior through sudden jumps between states located even at distant sites. This seems to be a general feature of non-Hermitian random systems. The relation of our findings to recent experimental results is also discussed.

Finally, we will investigate the propagation of Gaussian beams through such waveguide lattices characterized by correlated non-Hermitian disorder. In the context of non-Hermitian Photonics, it was recently demonstrated that is possible to suppress the effects of localization and thus achieve perfect transmission by considering correlated non-Hermitian disorder. In particular, one can derive a novel class of waves that have constant intensity (CI-waves) everywhere in space, even inside the scattering area [90, 91]. In the framework of coupled mode theory, we will demonstrate how the imaginary part of the refractive index needs to be adjusted to achieve perfect beam transmission, despite the presence of disorder. Remarkably, the effects of both diagonal and off-diagonal disorder in the waveguides and their couplings can be efficiently eliminated by our non-Hermitian design.

Chapter 2

One-dimensional Anderson model

In this chapter, we make a brief introduction to the concepts of Anderson localization and wave propagation in complex media, both in (quasi) 1-D systems. We formulate the mathematical description of these problems and present the main numerical techniques we used to obtain this thesis' results.

2.1 Tight-binding Hamiltonian

In this section we will consider the tight-binding Hamiltonian in 1-D and study its spectral properties (eigenvalues, eigenvectors and density of states), as well as the dynamical evolution of wavepackets in lattices described by it.

The tight-binding Hamiltonian operator is defined as:

$$\hat{\mathrm{H}}_{\mathrm{TB}} \equiv \sum_{n} \epsilon_n \left|n\right\rangle \left\langle n\right| + \sum_{\langle n,m\rangle} c_{n,m} \left|n\right\rangle \left\langle m\right| \ . \tag{2.1}$$

In the above, the first term expresses the on-site interaction of strength ϵ_n, which (ϵ_n) is called the site element of the n^{th} site and may have a different physical meaning depending on the specific characteristics of the system we consider. Since in this thesis we are interested in studying photonic waveguide lattices, the waveguides' propagation constants play the role of site elements in our case. On the other hand, the second term expresses the nearest neighbor hoping (summation over nearest neighbors $\langle n, m\rangle$), with $c_{n,m}$ being the coupling coefficient between the sites n, m.

In most of the cases that will concern us here, $c_{n,m} = \text{const.}\ \forall n, m$; then we can set $c_{n,m} = 1$ without loss of generality. In addition, if $\epsilon_n = \text{const.}$ $\forall n$, then the system becomes periodic and we can set $\epsilon_n = 0$ (again without

losing any generality). The tight-binding Hamiltonian $\hat{\mathrm{H}}_0$ of a 1-D periodic lattice with N sites in total, is a tridiagonal matrix of the form:

$$(\hat{\mathrm{H}}_0)_{n,m} = \delta_{n,m+1} + \delta_{n+1,m} \Rightarrow \hat{\mathrm{H}}_0 = \begin{pmatrix} 0 & 1 & 0 & \cdots & b_c \\ 1 & 0 & 1 & \cdots & 0 \\ \vdots & \ddots & \ddots & \ddots & \vdots \\ \vdots & \ddots & \ddots & \ddots & \vdots \\ b_c & \cdots & 0 & 1 & 0 \end{pmatrix}_{N\times N} \tag{2.2}$$

where in the above, $b_c = 0$ for closed (Dirichlet) and $b_c = 1$ for periodic boundary conditions. In this thesis we examine only the case of closed boundary conditions ($b_c = 0$).

On the other hand, the Hamiltonian $\hat{\mathrm{H}}$ of the 1-D Anderson model reads:

$$\begin{aligned} \hat{\mathrm{H}}_{n,m} = \delta_{n+1,m} + \delta_{n,m+1} + \epsilon_n \delta_{n,m} = (\hat{\mathrm{H}}_0)_{n,m} + \epsilon_n \delta_{n,m} \Rightarrow \\ \Rightarrow \hat{\mathrm{H}} = \begin{pmatrix} \epsilon_1 & 1 & 0 & \cdots & 0 \\ 1 & \epsilon_2 & 1 & \cdots & 0 \\ \vdots & \ddots & \ddots & \ddots & \vdots \\ \vdots & \ddots & \ddots & \ddots & \vdots \\ 0 & \cdots & 0 & 1 & \epsilon_N \end{pmatrix}_{N\times N} \end{aligned} \tag{2.3}$$

where ϵ_n = random $\in [-\frac{W}{2}, \frac{W}{2}]$ (uniform distribution), with W defined as the disorder strength/amplitude.

One can obtain the system's eigenvalues and eigenvectors via exact matrix diagonalization. The eigenstates of the Anderson Hamiltonian become more and more localized as we raise the value of W; something that can be clearly seen in Fig. 2.1.

Given the eigenvalues of the system, one can easily find (numerically) the density of states (DOS) as follows: we first sort the eigenvalues in ascending order and then make a histogram of Nb bins, where $1 \ll Nb \ll N$. For disordered systems, one needs to consider a large number of different realizations and sort all of their eigenvalues in ascending order, in order to get better results. After this procedure, one obtains the DOS by diving the histogram values over (i) the number of realizations, (ii) the bin spacing and (iii) the Hamiltonian's dimension N.

In Fig. 2.2 we show the system's DOS for (a) $W = 0$ and (b) $W = 1$. In the periodic case we also compare our result with the corresponding theoretical expression:

$$\mathrm{DOS}(\omega) = \frac{1}{\pi\sqrt{4-\omega^2}} \ . \tag{2.4}$$

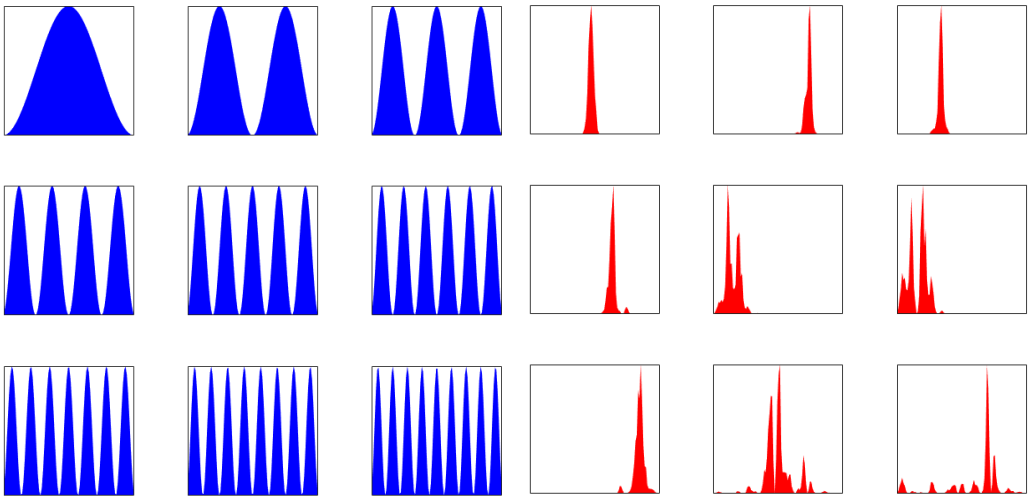

(a) W=0 (b) W=1

Figure 2.1: Intensity profiles of the first 9 eigenstates of the 1-D Anderson Hamiltonian with $N = 100$ and (a) $W = 0$, (b) $W = 1$.

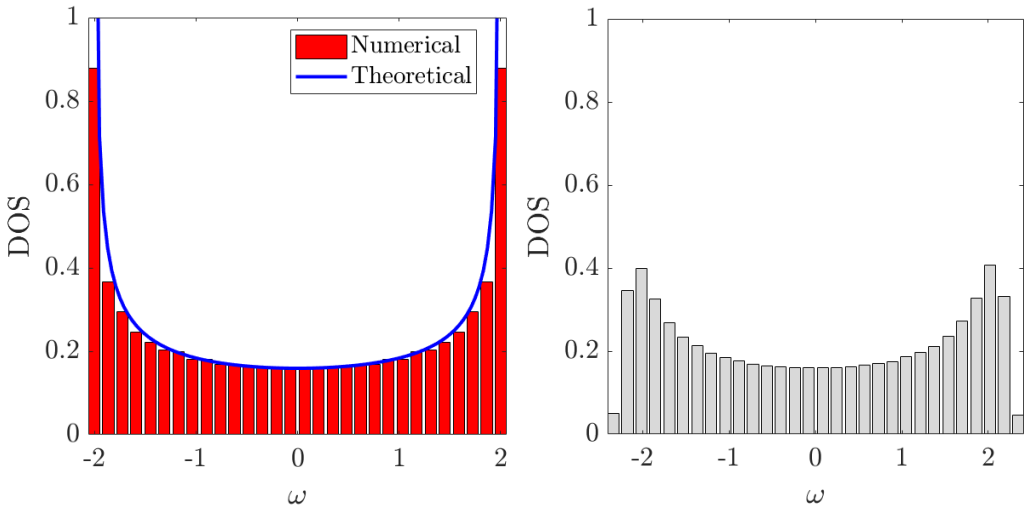

(a) W=0 (b) W=1

Figure 2.2: Density of states for the 1-D Anderson model with (a) $W = 0$ (analytical expression with blue line) and (b) $W = 1$. The y-axis scale is kept the same between (a) and (b) for comparison.

Knowing the system's Hamiltonian one can also study the dynamic evo-

lution of an initial wavefunction. This evolution is governed by the following set of coupled Schrodinger-like equations:

$$i\frac{\partial\psi}{\partial z} + \hat{\mathrm{H}}\psi = 0 \Leftrightarrow i\frac{\partial\psi_n}{\partial z} + (\psi_{n+1} + \psi_{n-1}) + \epsilon_n\psi_n = 0 \ , \tag{2.5}$$

which in the context of Photonics are called normalized coupled mode equations and describe the paraxial wave propagation in a 1-D waveguide array of N coupled channels, such as the one in Fig. 1.3.

In Eq. 2.5, z is the normalized propagation distance (which plays the role of time in quantum mechanics), while ψ_n and ϵ_n are the envelope of the electric field and the propagation constant (site element) of the n^{th} channel, respectively. Also $\psi \equiv (\psi_1 \ \psi_2 \ ... \ \psi_N)^T$. For more details regarding these equations and their normalization please see [71].

We solve Eq. 2.5 using a 4^{th} order Runge-Kutta algorithm [92]: we first discretize the z-vector: $z \to \{z_j\}$, where $z_j \equiv z_0 + j \cdot dz$, $j = 0, 1, .., M$, dz is the pseudo-time step (which we usually take $dz = 0.1$), and z_0 is the initial value of z which we take $z_0 = 0$.

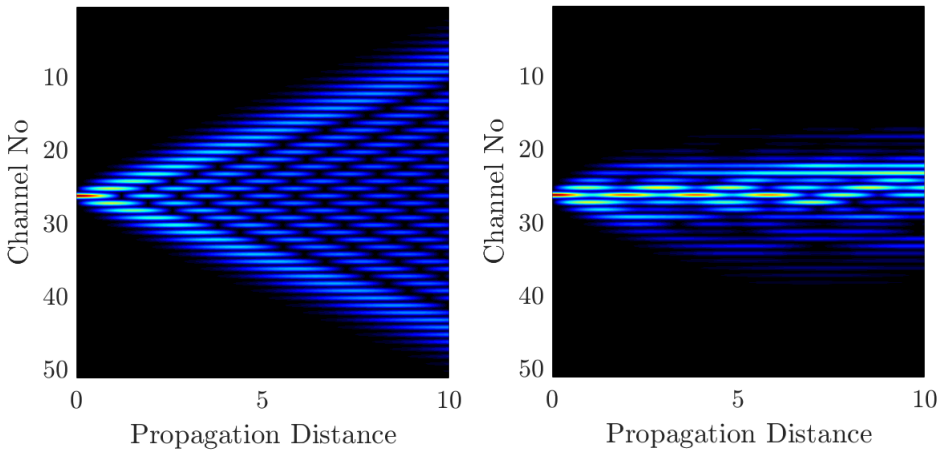

Figure 2.3: Field amplitude $|\psi_n(z)|$ z-evolution. Here we consider a single-channel excitation $\psi_n^0 = \delta_{n,n_0}$ in the middle of an Anderson lattice with $N = 51$ sites and for (a) $W = 0$ and (b) $W = 5$.

Given an initial wavefunction $\psi(z = 0) \equiv \psi^0$, we can simulate its propagation as follows: at first we start a loop running over the pseudo-time vector $j = 0 \to M - 1$. Denoting the wavefunction after the j^{th} step by ψ^j, in each

z-step we follow the procedure described below:

$$\begin{aligned}\phi = \psi^j \rightarrow \kappa_1 = idz \cdot \hat{\mathrm{H}}\phi \rightarrow \phi = \psi^j + \frac{\kappa_1}{2} \rightarrow \kappa_2 = idz \cdot \hat{\mathrm{H}}\phi \rightarrow \\ \rightarrow \phi = \psi^j + \frac{\kappa_2}{2} \rightarrow \kappa_3 = idz \cdot \hat{\mathrm{H}}\phi \rightarrow \phi = \psi^j + \kappa_3 \rightarrow \\ \rightarrow \kappa_4 = idz \cdot \hat{\mathrm{H}}\ \phi \rightarrow \psi^{j+1} = \psi^j + \frac{\kappa_1 + 2\kappa_2 + 2\kappa_3 + \kappa_4}{6}\ .\end{aligned} \tag{2.6}$$

In Fig. 2.3 we show the dynamic evolution of an initial single channel (delta) excitation in the middle site n_0 of an Anderson lattice: $\psi_n^0 = \delta_{n,n_0}$, for $W = 0$ and $W = 5$. We can observe the so-called "absence of diffusion" (absence of diffraction in our case) for $W > 0$, where localization takes place.

For an infinite periodic lattice, the analytical solution for the propagation of $\psi_n^0 = \delta_{n,n_0}$ is given by the following relation:

$$\psi_n(z) = i^{n-n_0} J_{n-n_0}(2z) \tag{2.7}$$

where J_n is the Bessel function of the first kind.

We define D as the difference between the field shown in Fig. 2.3(a) and the field given by Eq. 2.7:

$$D_n(z) \equiv |\psi_n^{num}(z) - \psi_n^{anal}(z)|\ . \tag{2.8}$$

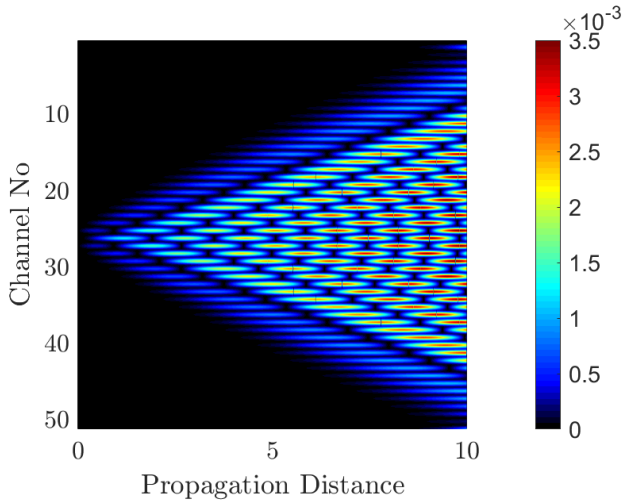

Figure 2.4: Plot of D_n (difference between the field shown in Fig. 2.3(a) and the field given by Eq. 2.7) as a function of propagation distance z.

Note that D is not exactly the numerical error since the numerical results correspond to a finite and not an infinite lattice. The plot of D as a function

of z is shown in Fig. 2.4. We can observe that D increases for larger values of z, since the effects of the boundaries become more and more significant. Nevertheless, the two results are really close.

2.2 T-Matrix

In this section, we consider the scattering problem shown in Fig. 2.5: an infinite lattice consisting of two periodic semi-infinite sublattices and a finite disordered sublattice of N sites in the middle region, as well as an incident Bloch wave coming from the right sublattice. The whole analysis of this section is based on chapter 7 of [28].

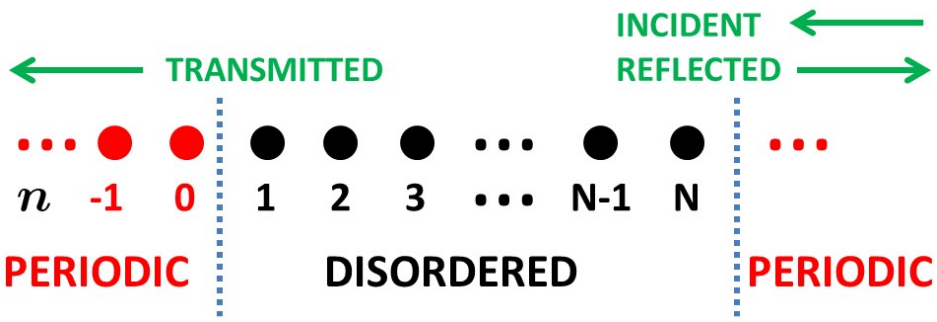

Figure 2.5: Setup of the scattering problem studied in this section. We consider an infinite tight-binding lattice consisting of three different sublattices: the middle one is finite and disordered (black color) and the two others are semi-infinite and periodic (red color). An incident Bloch wave coming from the right sublattice is considered.

To begin with, the site element distribution of the lattice is the following:

$$\epsilon_n = \begin{cases} \text{random} \in [-\frac{W}{2}, \frac{W}{2}] & \text{if} \quad 1 \leq n \leq N \\ 0 \quad \text{otherwise,} \end{cases} \tag{2.9}$$

where $W \geq 0$ is defined as the strength of disorder. Our goal is to find the wavefunction's values $\{\psi_n\}$ at the corresponding lattice sites $\{n\}$.

As seen in Fig. 2.5, at $n = 0$ we have only an outgoing (transmitted) wave and due to Bloch's theorem we get:

$$\psi_0 = 1 \quad \text{and} \quad \psi_{-1} = e^{-ik}\psi_0 = e^{-ik} \ , \tag{2.10}$$

where k is the Bloch momentum (we have set the lattice constant equal to 1). The Bloch momentum is related to the wave's eigenvalue ω according to the following dispersion relationship:

$$\omega = 2\cos k = e^{ik} + e^{-ik}. \tag{2.11}$$

Now, the tight-binding relation 2.5 provides us with:

$$\omega\psi_n = \epsilon_n\psi_n + (\psi_{n-1} + \psi_{n+1}) \ . \tag{2.12}$$

By rewriting the above equation we obtain the following recursive relation:

$$\psi_{n+1} = (\omega - \epsilon_n)\psi_n - \psi_{n-1} \tag{2.13}$$

or in matrix form:

$$\begin{pmatrix} \psi_{n+1} \\ \psi_n \end{pmatrix} = \begin{pmatrix} \omega - \epsilon_n & -1 \\ 1 & 0 \end{pmatrix} \begin{pmatrix} \psi_n \\ \psi_{n-1} \end{pmatrix} \equiv \hat{T}_n \begin{pmatrix} \psi_n \\ \psi_{n-1} \end{pmatrix} \tag{2.14}$$

where $\hat{T}_n$ is the so-called transfer matrix of the n^{th} site.

Thus, the coefficients ψ_N, ψ_{N-1} can be found in terms of the already known ψ_0, ψ_{-1} using the following relation:

$$\begin{pmatrix} \psi_N \\ \psi_{N-1} \end{pmatrix} = \prod_{n=0}^{N-1} \hat{T}_n \begin{pmatrix} \psi_0 \\ \psi_{-1} \end{pmatrix} \equiv \hat{T} \begin{pmatrix} \psi_0 \\ \psi_{-1} \end{pmatrix} \tag{2.15}$$

with $\hat{T}$ being the total transfer matrix of the disordered region.

We are now able to calculate various interesting features of the system. The localization length is one of them.

Generally speaking, the localization length ξ (in units of the lattice spacing) of a wave traveling in an infinite disordered lattice is defined as:

$$\xi \equiv -\lim_{n\to\infty} \frac{n}{\ln|\psi_n|} \ . \tag{2.16}$$

In practice, in order to calculate the localization length ξ corresponding to the eigenvalue ω, we first need to find the average wavefunction amplitude defined as:

$$\ln|\Psi_n| \equiv \langle \ln|\psi_n| \rangle \tag{2.17}$$

where an average over a large number (typically $\geq 5N$) of realizations is needed to obtain reliable results. In this case, $|\Psi_n|$ is directly related to ξ:

$$|\Psi_n| \propto e^{n/\xi} \ . \tag{2.18}$$

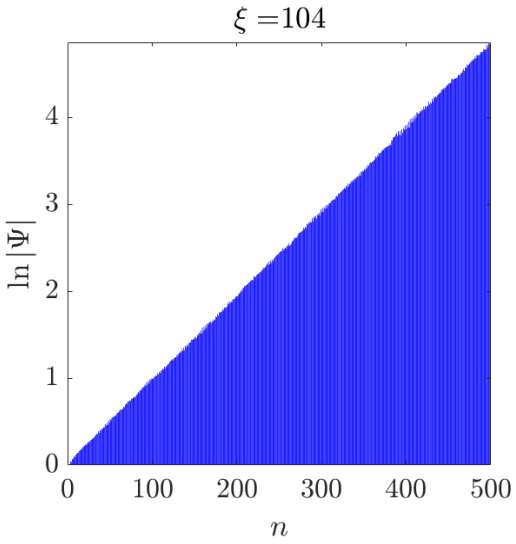

Figure 2.6: $\ln|\Psi|$ defined by Eq. 2.17 as a function of the site number, for $W = 1$ and $\omega = 0$ (band's center). The localization length ξ (in units of lattice spacing α) is shown in the graph's title.

Note that the most commonly used " $-$ " sign has been replaced by " $+$ " since here we considered a wave traveling from right to left.

So, in order to calculate the localization length, we need to plot the relation $n - \ln|\Psi|$ and perform a linear fitting:

$$\ln|\Psi| = A \cdot n + B \Rightarrow \xi = \frac{1}{A} \ , \tag{2.19}$$

as seen in Fig. 2.6.

Also, the wave's transmittance T is given by the formula:

$$\mathrm{T} = \frac{4\sin^2(k)}{|e^{ik}\psi_N - \psi_{N-1}|^2} \tag{2.20}$$

and is related to the localization length as follows:

$$\langle \ln \mathrm{T} \rangle = -\frac{2N}{\xi} \ . \tag{2.21}$$

In Fig. 2.7 we show plots of the transmittance T for various realizations of disorder and for two different values of W.

Finally, in the limit of weak disorder ($W \leq 1$) the localization length is approximately given by:

$$\xi(\omega) \simeq \frac{24(4-\omega^2)}{W^2} \ . \tag{2.22}$$

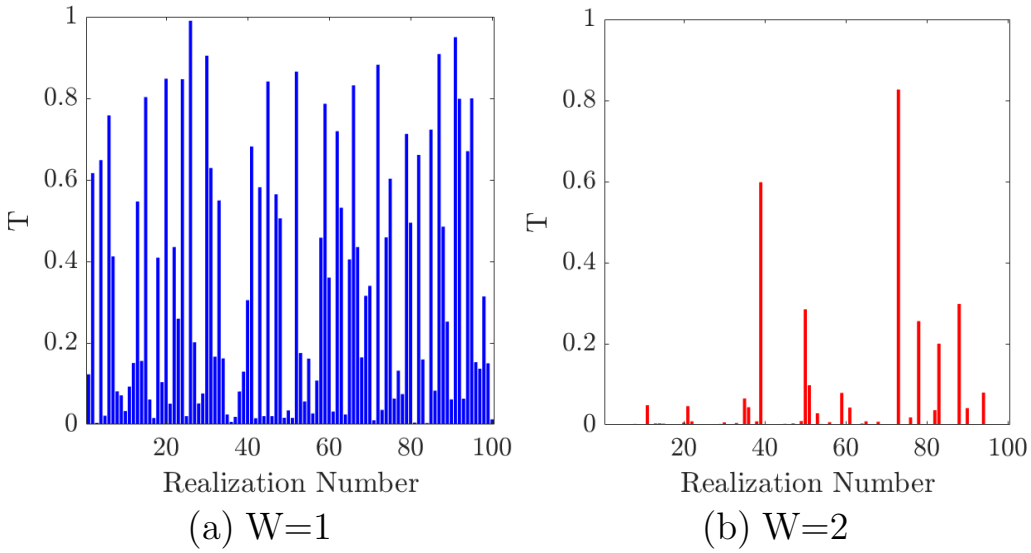

Figure 2.7: Transmittance T for different realizations of disorder. The system's size is taken $N = 100$ and the calculation has been performed for (a) $W = 1$ and (b) $W = 2$.

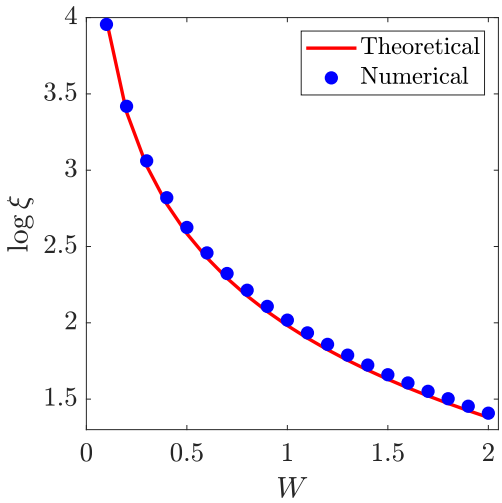

Figure 2.8: Logarithm (base 10) of the localization length ξ as a function of the disorder's strength W for $\omega = 0$. Numerical results (blue dots) are compared to the approximate theoretical prediction of Eq. 2.22 (red line).

In Fig. 2.8 we compare the approximate theoretical expression of Eq.2.22 with our numerical results, finding that they are in satisfactory agreement.

Chapter 3

Two-dimensional Anderson model

Here we examine the effects of uniform Hermitian and non-Hermitian disorder in 2-D waveguide lattices. In Sec. 3.1 we present and discuss some of the well known properties of 2-D Hermitian disordered systems. Subsequently, in Sec. 3.2, we introduce the 2-D non-Hermitian Anderson model and provide a systematic study of the interplay between disorder and non-Hermiticity. More specifically, we study the system's eigenspectrum in the complex frequency plane, as well as the localization properties of its eigenstates, either by the participation ratio or the level spacing, defined in the complex plane.

3.1 Hermitian disordered lattice

In this section we will study the effects of real disorder in 2-D tight-binding lattices of $N \times N$ sites and with site element distribution $\{\epsilon_{p,q}\}, (p, q = 1, ..., N)$.

In the case of a square waveguide lattice, the coupled-mode equations of Eq. 2.5 become:

$$i\frac{\partial \psi_{p,q}}{\partial z} + (\psi_{p+1,q} + \psi_{p-1,q} + \psi_{p,q+1} + \psi_{p,q-1}) + \epsilon_{p,q}\psi_{p,q} = 0 \ . \tag{3.1}$$

A schematic of our system is shown in Fig. 3.1(a).

In order to find the eigenmodes of the system, we perform the substitution $\psi_{p,q} = \phi_{p,q} \cdot \exp(-i\omega_j z)$ in Eq. 3.1 and obtain the following eigenvalue problem:

$$\omega_j \phi_{p,q} = (\phi_{p+1,q} + \phi_{p-1,q} + \phi_{p,q+1} + \phi_{p,q-1}) + \epsilon_{p,q}\phi_{p,q} = \hat{\mathrm{H}}\phi_{p,q} \tag{3.2}$$

where ω_j is the eigenvalue of the j^{th} eigenmode, with $j = 1, 2, ..., N^2$ and $\hat{\mathrm{H}}$ is the Hamiltonian of the 2-D Anderson model, which reads:

$$\hat{\mathrm{H}}_{n,m} = \epsilon_n \cdot \delta_{n,m} + (\hat{\mathrm{H}}_0 \otimes \hat{\mathbb{1}} + \hat{\mathbb{1}} \otimes \hat{\mathrm{H}}_0)_{n,m} \tag{3.3}$$

with $\hat{\mathrm{H}}_0$ being the 1-D tight-binding Hamiltonian of Eq. 2.2 and $\{\epsilon_n\}$ the elements of the $N^2 \times 1$ column vector, occurring from the stretching of the site element matrix $\{\epsilon_{p,q}\}$. Also, $\otimes$ denotes the Kronecker tensor product between two matrices and the matrix $\hat{\mathrm{H}}$ has dimension $N^2 \times N^2$.

For the periodic case ($\epsilon_{p,q} = 0\ \forall p, q$), we show plots of the field amplitude of the nine lowest-eigenvalue eigenmodes, in Fig. 3.1(b). Note that we are assuming Dirichlet boundary conditions as always.

We are interested in finding how these eigenmodes and eigenvalues change when the system becomes disordered. For the disordered case, we consider once again a uniform site element distribution: $\epsilon_{p,q} \in [-\frac{W}{2}, \frac{W}{2}]$, where W is the strength of disorder.

In Figs. 3.1(c),(d), we present the nine lowest-eigenvalue eigenmodes for the case of (c) weak disorder with $W = 0.5$ and (d) strong disorder with $W = 5$. As expected, the eigenstates become more and more localized as W increases. However, contrary to the 1-D case, in Fig. 3.1(c) one may observe that the amplitude patterns, despite being distorted, do not seem spatially confined. This is a consequence of the fact that in 2-D the localization length is $\xi_{2D} \propto le^{kl}$, where l is the mean free path. This relation implies that, even though all states are localized for any value of W, if the strength of disorder is weak the localization length becomes so large that $\xi_{2D} \gg$ system's size, thus leading to the misconception that the eigenstates are extended. This issue troubled the Physics community for quite some time in the past [93].

Moving on, the DOS of a 2-D periodic square lattice is given by [14]:

$$\mathrm{DOS}(\omega) = \frac{1}{2\pi^2} K[\sqrt{1 - \frac{\omega^2}{16}}], \tag{3.4}$$

where K is the complete elliptic integral of the first kind, defined as:

$$K(x) \equiv \int_0^1 \frac{dt}{\sqrt{(1-t^2)(1-x^2t^2)}}\ . \tag{3.5}$$

For zero disorder the DOS exhibits at both band edges a discontinuity, as well as a logarithmic singularity at the band's center (the latter is not easily captured numerically). These non-smooth points are also called van-Hove singularities. Our numerical result, together with the theoretical curve of Eq. 3.4, are shown in Fig. 3.2(a).

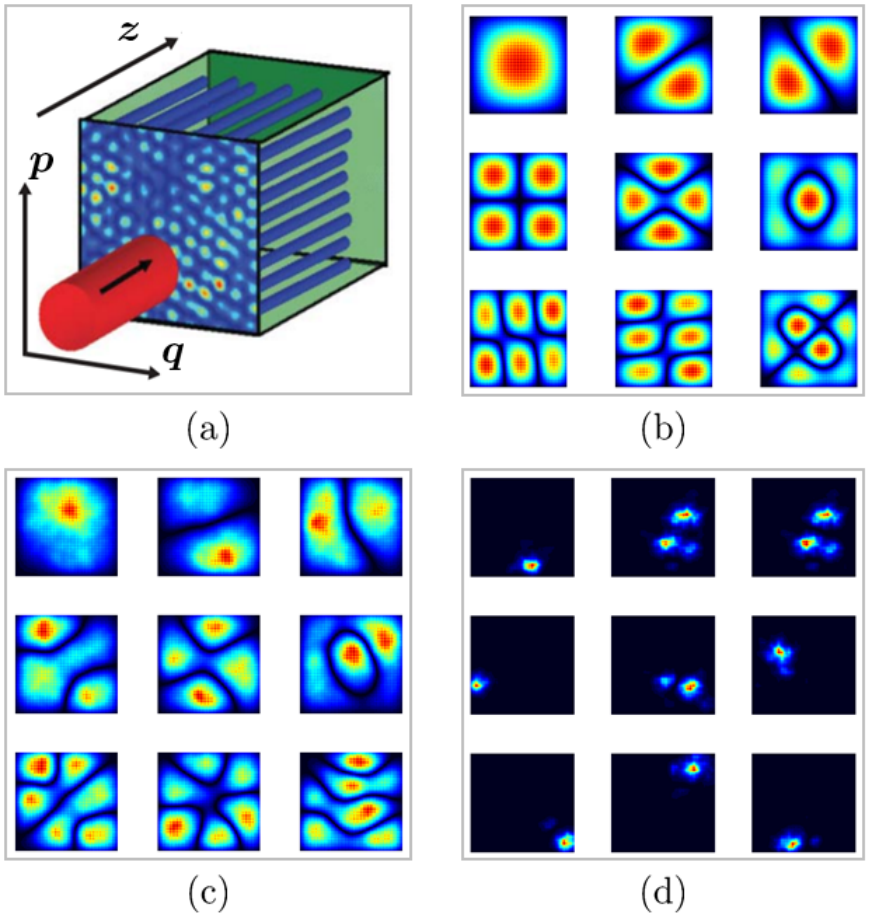

Figure 3.1: (a) Schematic representation of a square waveguide lattice. The wave evolution along the z-axis is described by Eq. 3.1. A probe beam entering the lattice is also presented (figure taken from the experimental work [24]). (b)-(d) Field amplitude for the nine lowest-eigenvalue eigenmodes of a disordered square lattice with 30×30 waveguides and for: (b) $W = 0$ (periodic case), (c) $W = 0.5$ (weak localization regime) and (d) $W = 5$ (strong localization regime). In subfigures (b)-(d), a shading-interpolation has been performed for illustration purposes.

We also present the corresponding DOS of the 2D Anderson model with $W = 2$, in Fig 3.2(b). Now we can observe that the introduction of disorder eliminates all of the aforementioned van-Hove singularities and makes the curve smoother in general. Aside from this difference though, the resulting DOS has a similar form to the one in Fig. 3.2(a).

Another physical quantity of interest is the so-called level spacing distri-

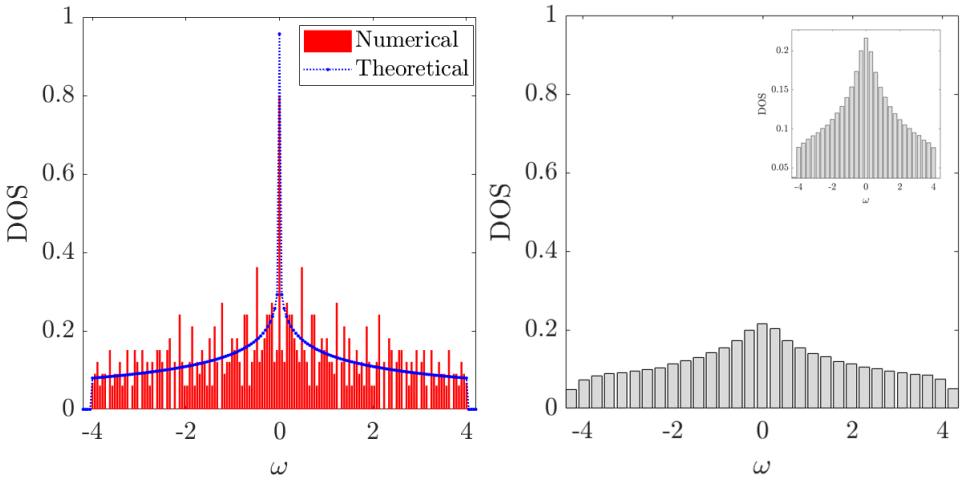

Figure 3.2: DOS of a 2-D square lattice: (a) Periodic system (comparison between theoretical and numerical results), (b) Anderson model with $W = 2$. The y-axis scale is kept the same between (a) and (b) for comparison. Inset: zoom of (b).

bution $\mathrm{P}(s)$, where s represents the normalized nearest-neighbor eigenvalue spacing defined as:

$$s_n \equiv \frac{\Delta\omega_n}{\langle \Delta\omega_n \rangle}, \quad \text{where} \quad \Delta\omega_n \equiv \omega_n - \omega_{n-1} \ , \tag{3.6}$$

assuming that the eigenvalues are ordered in the ascending order ($\omega_n \geq \omega_{n-1}$). This distribution often takes one of several universal forms, depending only on the disorder strength and not on the specific details of the medium [94, 95]. In particular, for weak disorder the modes are extended over the whole disordered area and $\mathrm{P}(s)$ approximately obeys the Wigner-Dyson distribution [Fig. 3.3(a)]:

$$\mathrm{P}_{WD}(s) = \frac{\pi s}{2} \exp(-\frac{\pi s^2}{4}) \ . \tag{3.7}$$

We have to note here that the most significant property of $\mathrm{P}(s)$ in this case is the so-called level repulsion phenomenon: $\mathrm{P}(0) = 0$. This feature is a consequence of the extended character of the system's eigenmodes, since the latter overlap in space and thus cannot posses the same eigenvalue, given their mutual orthogonality property.

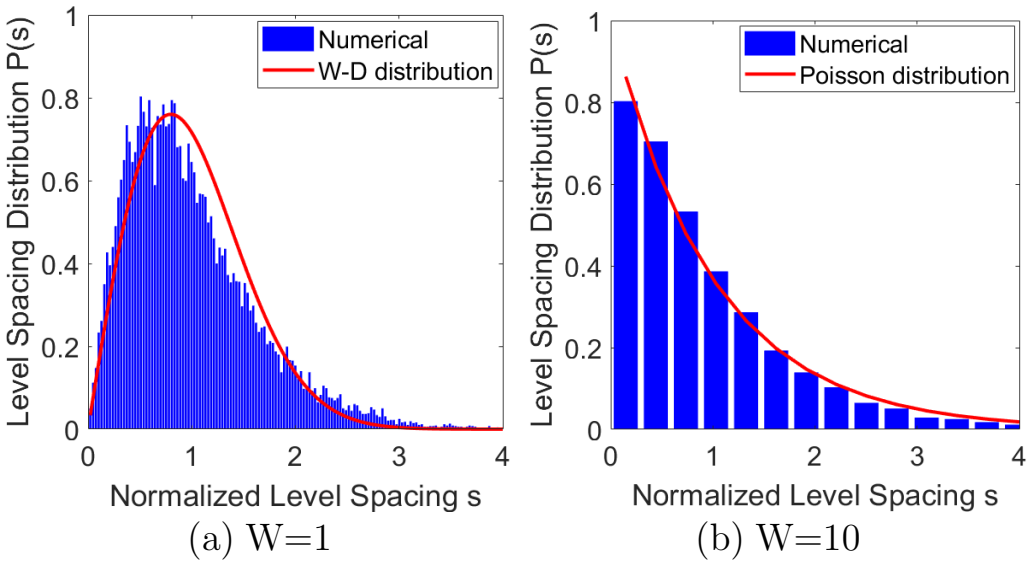

Figure 3.3: Histogram of normalized level spacing for (a) $W = 1$ and (b) $W = 10$ (blue bars). The red lines show the corresponding theoretical prediction.

On the other hand, in the strong disorder regime, $\mathrm{P}(s)$ approaches the Poisson distribution given by [Fig. 3.3(b)]:

$$\mathrm{P}_P(s) = \exp(-s) \ . \tag{3.8}$$

We can see that in this case $\mathrm{P}(0) \neq 0$, implying that the eigenvalues can now come arbitrarily close to each. Again, this is directly related to the localized nature of the corresponding eigenmodes, which may now posses zero overlap and thus be completely uncorrelated.

We also have to note that in the intermediate cases (between weak and strong disorder), the obtained distribution is a linear combination of the Wigner-Dyson and Poisson distributions.

Finally, one can also study the diffraction pattern of an initial delta-excitation in the middle of a square lattice, again using the $RK4$ method, - the procedure described by Eqs. 2.6 - but with $\hat{\mathrm{H}}$ given by Eq. 3.3.

These diffraction patterns are shown in Fig. 3.4. In particular, in the left column we present the field's intensity output at $z = 6$ (a), and 3 intensity-snapshots (for $z = 2, 4$ and 6) of the propagation process (c), both for a periodic lattice ($W = 0$). In the right column we show plots of the corresponding results for a disordered lattice with $W = 5$ (strong localization regime). Once again, one can observe the absence of diffraction, as well as the random distribution of the fields intensity due to disorder.

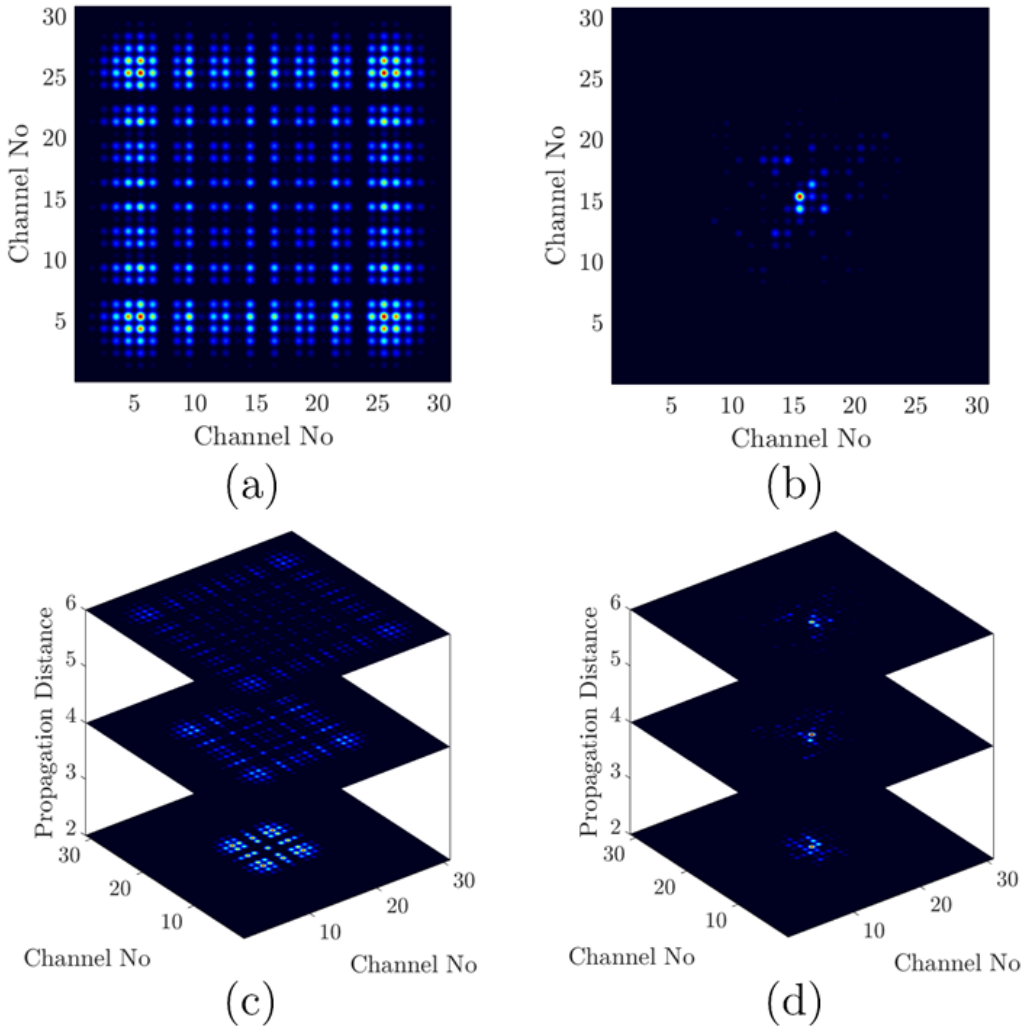

Figure 3.4: Left column: (a) field intensity output at $z = 6$ of an initial delta-excitation in the middle of a 31×31 square lattice, and (c) 3 snapshots ($z = 2, 4, 6$) of the diffraction process, both for a periodic lattice ($W = 0$). Right column: same as in (a) and (c), but for a disordered lattice with $W = 5$.

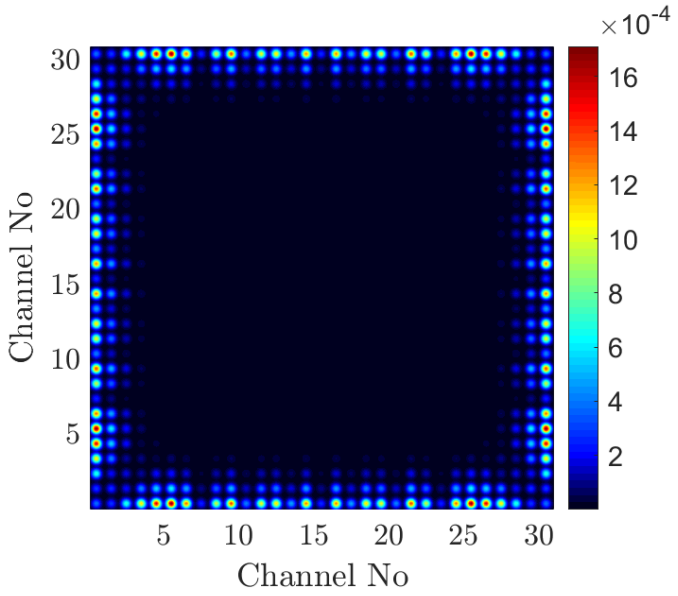

Figure 3.5: Plot of $D_{p.q}$ - which describes the difference between the numerical [Fig. 3.4(a)] and analytical (Eq. 3.9) solutions - defined by Eq. 3.10, for $z = 6$ and $N = 31$.

As in the 1-D case, there exists an analytical solution for the diffraction of a single-channel excitation in an infinite and periodic lattice: $\psi_{p,q}(0) = \delta_{p,p_0}\delta_{q,q_0}$. This solution is now a product of two Bessel functions and reads as follows:

$$\psi_{p,q}(z) = i^{p-p_0} i^{q-q_0} J_{p-p_0}(2z) J_{q-q_0}(2z) \ . \tag{3.9}$$

In order to compare our theoretical and numerical results, we use the extension of the function $D(z)$ (see Eq. 2.8) in 2 spatial dimensions, given by:

$$D_{p,q}(z) \equiv |\psi^{num}_{p,q}(z) - \psi^{anal}_{p,q}(z)| \ . \tag{3.10}$$

A plot of $D_{p,q}$ for a square lattice with $N = 31$, $z = 6$ and a single-channel excitation in its middle channel ($p = q = 16$) is shown in Fig. 3.5. Once again, the two results are really close and their difference increases as we move towards the boundaries, as expected.

3.2 Non-Hermitian disordered lattice

In this section we consider guided non-Hermitian structures, where $\epsilon_{p,q}$ are complex; this physically means that each waveguide is characterized by either gain ($\mathrm{Im}\{\epsilon_{p,q}\} < 0$) or loss ($\mathrm{Im}\{\epsilon_{p,q}\} > 0$) and by its real part $\mathrm{Re}\{\epsilon_{p,q}\}$. The Hamiltonian of the system is again given by Eq. 3.3, but with $\{\epsilon_i\}$ being complex this time. A schematic of our model is provided in Fig. 3.6.

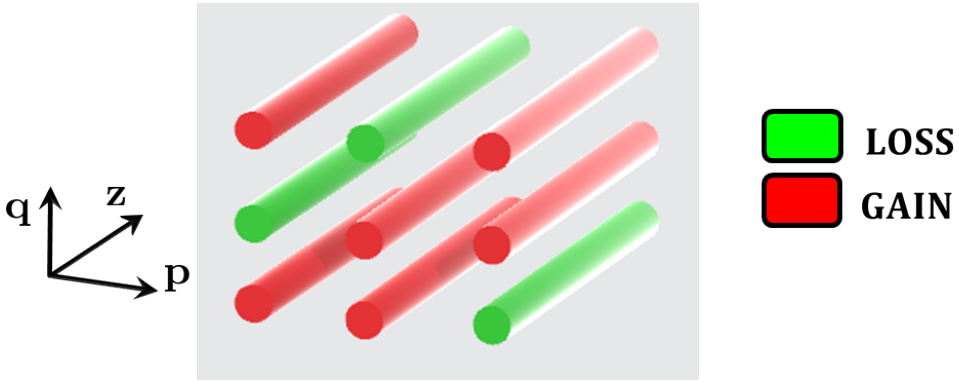

Figure 3.6: A schematic depiction of the physical system that we consider in this section: a 2-D waveguide lattice with random gain and loss.

Since $\hat{\mathrm{H}}$ is now a non-Hermitian matrix, it is fully described by a set of biorthogonal right $|\phi_j^R\rangle$ and left $|\phi_j^L\rangle$ eigenmodes. In other words, we have the following right eigenvalue problem:

$$\hat{\mathrm{H}}\,|\phi_j^R\rangle = \omega_j\,|\phi_j^R\rangle \tag{3.11}$$

and the corresponding left eigenvalue problem of the adjoint matrix:

$$\hat{\mathrm{H}}^\dagger\,|\phi_j^L\rangle = \omega_j^*\,|\phi_j^L\rangle \ . \tag{3.12}$$

The associated biorthogonality condition is $\langle\phi_j^L|\phi_i^R\rangle = \delta_{i,j}$. In general, the right and left eigenvectors are different and, since any dynamics of the problem include both the right and the left set of eigenfunctions, one needs to study both of them. In our case though, the left and right eigenfunctions are complex conjugate pairs since $\hat{\mathrm{H}}^\dagger = \hat{\mathrm{H}}^*$. This is a direct outcome of the corresponding one-dimensional matrices' $\hat{\mathbb{1}}, \hat{\mathrm{H}}_0$ Hermiticity.

We will examine phenomena related to Anderson localization in two different cases of non-Hermitian disorder: (a) imaginary disorder, where the potential strength is imaginary with a distribution of the form: $\epsilon = i\epsilon_I$, $\epsilon_I \in [-\frac{W}{2}, \frac{W}{2}]$ and (b) both real and imaginary disorder, where the potential strength is complex, $\epsilon = \epsilon_R + i\epsilon_I$ with $\epsilon_R \in [-\frac{W}{2}, \frac{W}{2}]$ and $\epsilon_I \in [-\frac{W}{2}, \frac{W}{2}]$.

A value indicative to the localization of the eigenmodes is the participation ratio of each mode (PR_j), which is defined by the relation:

$$PR_j \equiv \frac{|\sum_{i=1}^{N^2} |\phi_j(i)|^2|^2}{\sum_{i=1}^{N^2} |\phi_j(i)|^4} \tag{3.13}$$

where we have used the right eigenvectors and the sum includes all N^2 sites of the system. Generally speaking, the PR measures the spread of a state $|\phi\rangle$ over a basis $\{|i\rangle\}_{i=1}^{N^2}$. For weak disorder strength, PR takes values comparable to the system's area, as all lattice sites participate (almost) equally to the eigenfunction. For higher values of W, the PR decreases, which means that the eigenmodes tend to become more and more localized. At this point we have to emphasize that the participation ratios based on the left eigenvectors are exactly the same with the above, since $(|\phi_j^L\rangle)^* = |\phi_j^R\rangle$, according to our previous discussion.

We also define the extent length of each mode, which is an easily measured and convenient in some cases quantity, by the relation:

$$\lambda_j \equiv \frac{\sqrt{PR_j}}{2} \ . \tag{3.14}$$

To begin with, we will illustrate the eigenvalue spectrum of Eq. 3.1 in the complex eigenfrequency plane and superimpose the values of PR (of the corresponding eigenmodes) by denoting them with different colors. We do not present any results for the case of real n, since they are well known: For weak disorder the density of states (DOS) follows more or less the unperturbed DOS with the rounding of the discontinuities at the band edges and the logarithmic singularity at the band center; states remain essentially extended except at the extreme tails. For strong disorder, the DOS tends to follow the distribution of the potential strength and all states become strongly localized.

In Fig. 3.7, we show the calculated eigenvalue spectra in the complex frequency plane for various disorder strengths and relate the color of each eigenvalue with the logarithm of the corresponding participation ratio, as seen in the colorbar of the graphs. In this figure we restrict ourselves to only the cases of imaginary disorder (case (b), left column) and the case of disorder in both the real and the imaginary part of the potential (case (c), right column), and for three different disorder strengths.

We can observe that, on both cases, the eigenvalue spectrum forms an approximate ellipse on the complex plane, with a different ellipticity in each case. Note that the spectrum of a system with random diagonal and off-diagonal elements forms a circle on the complex plane. In our case, due to

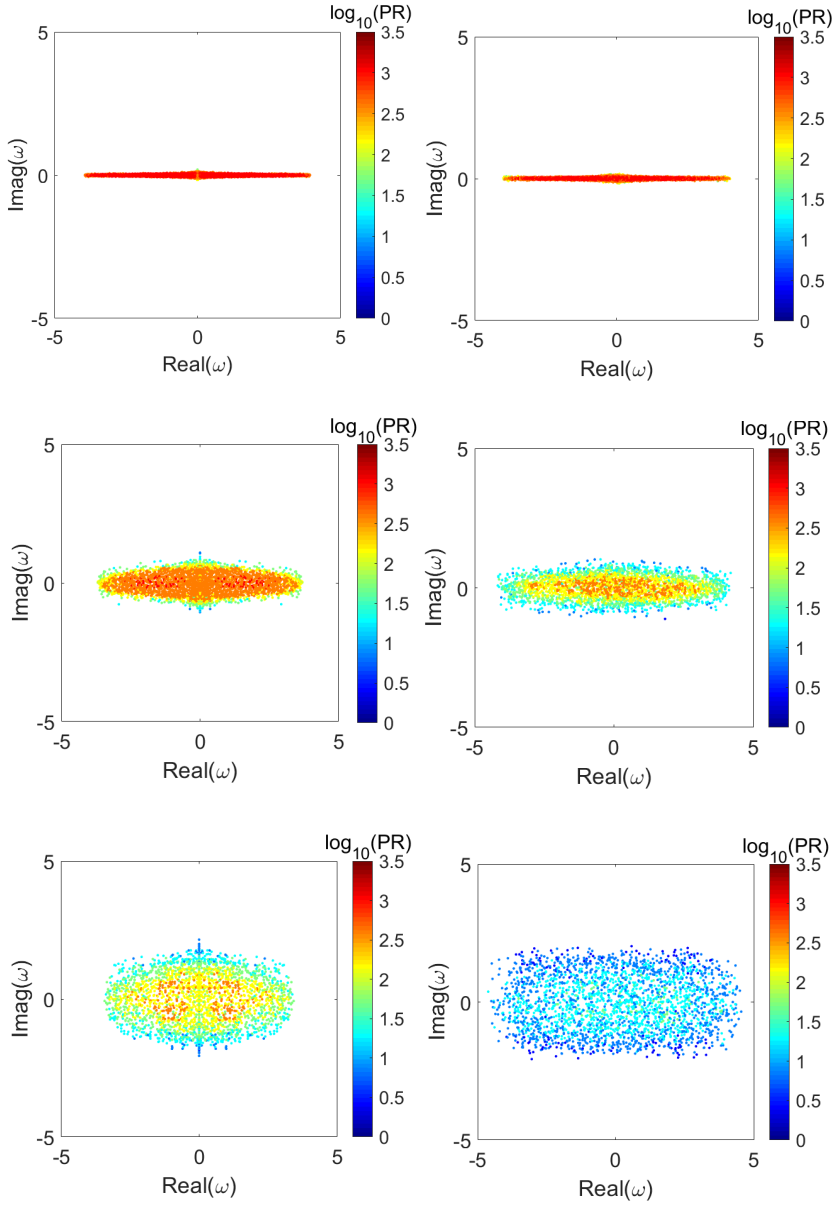

Figure 3.7: Eigenvalue spectra of a 50×50 waveguide lattice (2500 sites) in the complex frequency plane, for a particular realization of the random system and for various disorder strengths: (a) $W = 1$ (first row), (b) $W = 3$ (second row) and (c) $W = 5$ (third row). In the left column, disorder is applied only to the imaginary part of the potential strength, while $\mathrm{Re}(\epsilon_{p,q})$=0; in the right column, disorder of the same W is applied in both the real and the imaginary part of $\epsilon_{p,q}$. Note that the color of each eigenvalue is related to the participation ratio (spatial extension) of the corresponding eigenstate, as seen in the colorbar of the figures.

the lack of randomness in the couplings, the obtained spectrum is elliptical [96, 97]. As expected, the ellipse is widened for increasing disorder.

Most interestingly, we can also observe that, in general, the modes around the center of the elliptical pattern are the most extended ones, while the ones near it's edges are the most localized; this seems to be the non-Hermitian extension of the corresponding well known result from the case of real disorder, in which the eigenstates tend to become gradually localized as we move towards the edges of the bands.

Figure 3.7 provides a general semi-qualitative picture of the whole spectrum, as well as information about how extended (or localized) the corresponding eigenstates are. However, quantitative information about how dense the spectrum is in each sub-region of the complex frequency plane cannot be easily inferred from these plots. To remedy this missing information we consider first the density of states (DOS) in the complex frequency plane (averaged over realizations of the random system). To define the DOS we count the number of states δN_0 with eigenfrequencies located within an elementary square of area $\delta A = \delta\omega_R \times \delta\omega_I$ and centered at the point $\omega = \omega_R + i\omega_I$ of the complex frequency plane; then we have by definition:

$$\mathrm{DOS}(\omega) \equiv \frac{\delta N_0}{\delta A} \ . \tag{3.15}$$

Usually, we implicitly assume that the DOS is averaged over many realizations of the random system. The DOS, as expected, depends on the disorder strength. For small values of disorder, all the eigenvalues are concentrated near the real axis, while their density is higher in the center and decays as we move towards the edges of the spectrum (as in Fig. 3.2). On the other hand, for the case of strong disorder, the eigenvalues become almost uniformly distributed in the whole spectrum and tend to follow the same distribution as the diagonal matrix elements, in the limit $W \gg V$, where V is the coupling coefficient (the DOS at the edges drops to zero not discontinuously in contrast to the matrix elements). Most interesting is the case of an intermediate value of disorder, which is shown in Fig. 3.8, for $W = 3$. In this plot we can observe that the DOS shows four weak peaks located on the real and the imaginary axis and near the edges of the spectrum. The peaks are found symmetrically over the center of the complex plane. In addition, the DOS appears to decay as we further move away from these two axis.

Regarding the level spacing statistics, there are several ways to define the level spacing, s, in the complex frequency plane. One way, termed "1" and for a particular realization of the disorder, is the following:

$$s_1(\omega) \equiv \sqrt{\frac{\delta A}{\delta N_0}} \tag{3.16}$$

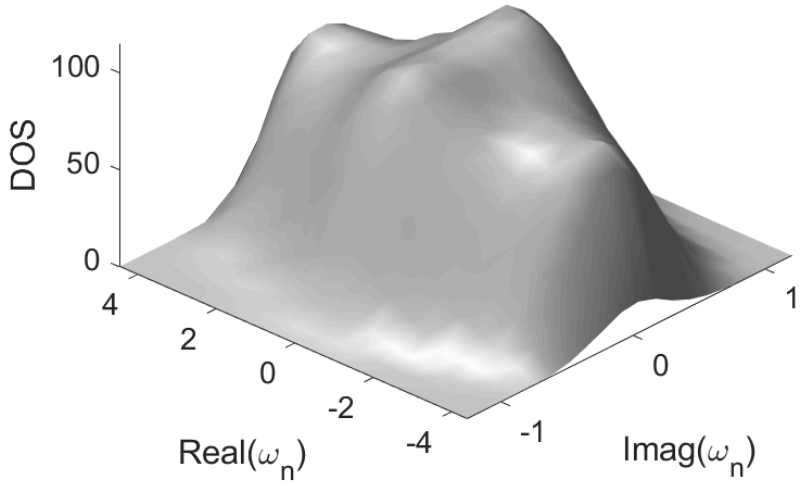

Figure 3.8: Density of states per unit area in the complex plane Real(ω)-Imag(ω), for the case of disorder in both the real and the imaginary part of the diagonal matrix elements and disorder strength $W = 3$. We have averaged over 1000 realizations of the disorder.

which is directly related with the DOS: $s = (\text{DOS})^{-\frac{1}{2}}$. (This direct relation between DOS and s acquires an extra numerical coefficient if both quantities are averaged over many realizations of the random system).

Another way, termed "2", to define the level spacing, s, which is the one most commonly used [96], at each eigenfrequency ω_j is as the minimum distance in the complex frequency plane between two neighboring eigenfrequencies averaged over many realizations of the disorder:

$$s_2(\omega_j) \equiv |\omega_j - \omega_{j-1}| \ . \tag{3.17}$$

In the above expression, ω_{j-1} is the eigenvalue which is nearest to the eigenvalue ω_j, on the real axis (Hermitian case) or on the complex plane (non-Hermitian case).

Definition 1 gives the nearest level spacing in the complex frequency plane averaged essentially over all directions in this plane; definition 2 gives the nearest level spacing along only one direction, the direction which at each eigenfrequency gives the minimum nearest level spacing. It is obvious that the second definition will result systematically in a smaller level spacing, as shown in Fig. 3.9. In Fig. 3.9(a) we plot the level spacing s, according to both definitions 1 and 2, for reasons of comparison, and for $W = 3$ in both the real and the imaginary part of the diagonal matrix elements, vs the real frequency axis (i.e. vs ω_R and for ω_I=0), while in Fig. 3.9(b) along the

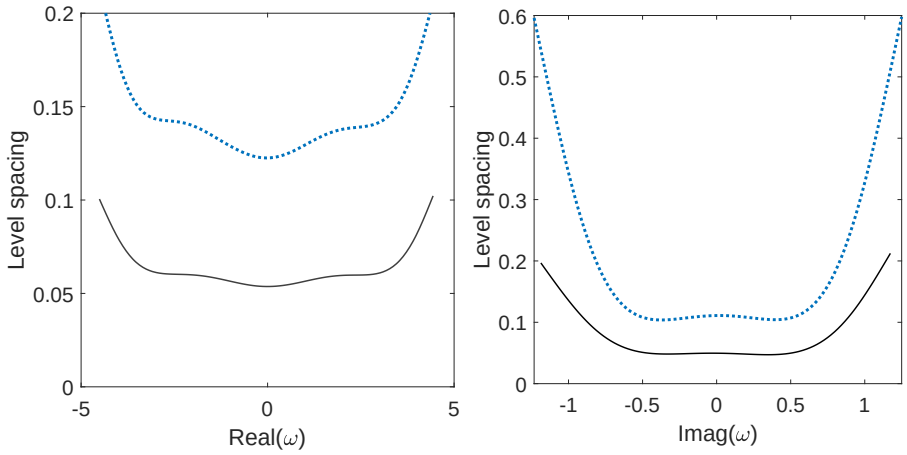

(a) s - Real(ω) (b) s - Imag(ω)

Figure 3.9: Level spacing s plotted along the real axis (a) and the imaginary axis (b) of the complex frequency plane Real(ω)-Imag(ω) and for the case of disorder in both the real and the imaginary part of the diagonal matrix elements and disorder strength $W = 3$. The blue dotted line represents results of calculations using the definition 3.16 of level spacing (s_1), while the black line represents results using definition 3.17 (s_2). An average over 1000 realization of disorder is performed in each case.

imaginary frequency axis, (i.e. vs ω_I and for ω_R=0).

We have to note that we deal with non-Hermitian matrices with complex spectra and as a result there is no unique definition of the level spacing, since the second or the third nearest neighbor eigenfrequency can be close to the first in the complex plane. The definition based on Eq. 3.16 is also a measure of the level spacing by being the square root of the area per eigenvalue in the complex plane (essentially averaging over the level spacings within this area); in contrast, the definition based on Eq. 3.17 picks the smaller among these level spacings, and as such is somehow smaller than but similar to that of Eq. 3.16. Thus the two different measures of level spacing lead to similar, but not identical, conclusions.

In Fig. 3.10 we present our results concerning the linear extent, λ, averaged over all the eigenmodes of the system, as a function of the disorder strength: $\lambda \equiv \langle \lambda_j \rangle$. We consider the three different cases: (1) disorder only in the real part of the diagonal matrix elements; (2) same disorder only in the imaginary, and (3) same disorder in both the real and the imaginary parts. The comparison of the three cases reveals a very interesting feature: While case (1), real disorder, exhibits a monotonic drop of the extent of

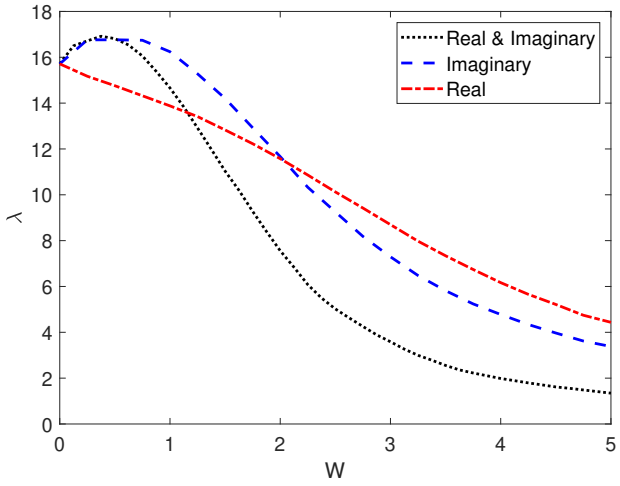

Figure 3.10: Mean extent length λ, averaged over the whole spectrum, as a function of the disorder strength W, for a lattice of 50×50 waveguides; uncorrelated disorder for all the three cases: Disorder only in the imaginary part of the diagonal matrix elements (blue dotted line), disorder only in the real part (red dash-dot line) and disorder of the same amplitude in both the real and the imaginary part (black dashed line).

the eigenfunctions with increasing disorder, as expected, cases (2) and (3), complex disorder, exhibit a surprising increase of the extent of the eigenfunctions with increasing disorder (for small disorder) before they eventually drop even faster than case (1). We attribute this anomaly for weak disorder to the fact that an imaginary part in the Hamiltonian breaks time reversal symmetry (TRS); it is well known that in Hermitian systems the breaking of TRS (usually by the presence of a static magnetic field) favors delocalization (see [93] pp. 510-513). In the present case imaginary disorder acts in a dual way: its implicit TRS breaking favors more extended states, while its disorder nature favors more localized states; the first aspect seems to dominate for only weak disorder, which is not actually surprising: for weak imaginary disorder its breaking of TRS is enough to randomize the phases of closed paths transversed in opposite directions; beyond this point the breaking of TRS has nothing to offer while the further increase of W contributes only to localization.

As mentioned earlier, the distribution of the level spacing averaged over the whole spectrum provides in the Hermitian case valid information [96] about the localization or not of the eigenfunctions. More specifically, when it comes to wave propagation in disordered media (either classical or quantum), this distribution is directly related with the spatial extent of the system's

modes.

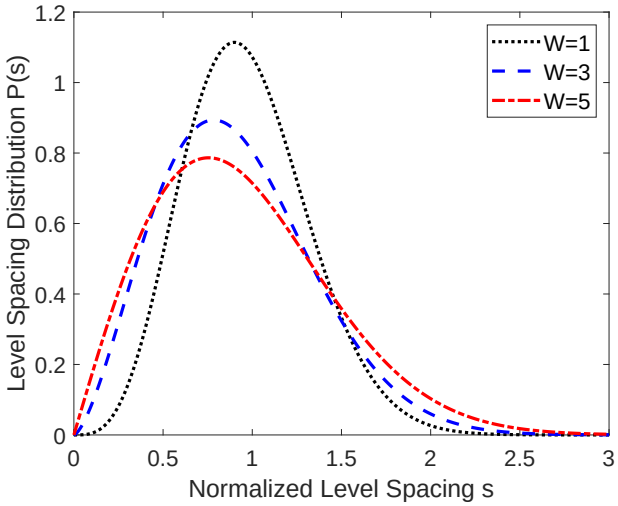

Figure 3.11: Probability density P of normalized level spacings s, as defined by Eq. 3.17, averaging over the whole spectrum. In this plot, disorder is applied in both the real and the imaginary part of the potential. The results for three values of disorder strength are shown: $W = 1$ (black dotted line), $W = 3$ (blue dashed line) and $W = 5$ (red dash-dot line). An ensemble of 50 realizations of disorder is used in each case.

When disorder is applied on the imaginary part of the potential though, the eigenvalue spacings (according to definition 2, Eq. 3.17) appear to obey a different probability distributions than the ones referred above. In Fig. 3.11 we show the level spacing distribution for the case of both real and imaginary disorder and for three different values of disorder strength ($W = 1$, $W = 3$ and $W = 5$). The results for only imaginary disorder do not differ significantly from the ones shown in the figure. We can observe that, for the above cases, the level spacing distribution can be described from a sub-Wigner (SW) probability distribution curve fitting:

$$\mathrm{P}_{SW}(s) = As^B \cdot \exp(-Cs^2), \quad B \geq 1 \ . \tag{3.18}$$

For $W = 1$, the exponent is $B \simeq 3$ and as we raise the disorder this exponent is gradually lowered (for $W = 3$, $B \simeq 1.5$). For $W = 5$, $B = 1$ and the level spacing distribution obeys the Wigner-Dyson probability distribution $\mathrm{P}_{WD}(s)$. Thus, we find that the level repulsion undergoes a smooth transition from s^3 to s^1 with increasing disorder; a similar behavior to the one found in random matrix theory papers, such as [98].

In the strong disorder regime ($W = 5$ in Fig. 3.11), we find that $\mathrm{P}(s) \simeq \mathrm{P}_{WD}(s)$. Since our level statistics take place in the 2-D complex plane, this distribution expresses the Poissonian statistics of uncorrelated eigenvalues located in 2 spatial dimensions [99, 100].

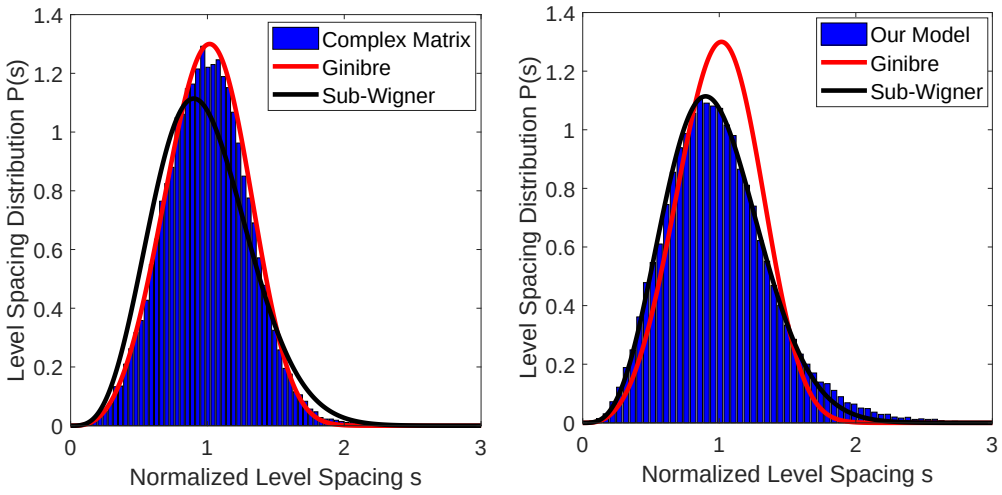

Figure 3.12: Probability densities P of normalized level spacings s, as defined in Eq. 3.17, averaged over the whole spectrum for disorder strength $W = 1$ and for the same size. (a) P(s) for a full complex matrix with random elements (blue) compared with Ginibre (red) and sub-Wigner (black). (b) P(s) for our model (blue) compared with Ginibre (red) and sub-Wigner (black). An ensemble of 50 realizations of disorder is used in each case.

On the other hand, in the case of weak disorder ($W = 1$), the level spacing distribution is a sub-Wigner one which exhibits cubic level repulsion [$\mathrm{P}(s) \sim s^3$ as $s \to 0$]. Since this dependence is similar to the corresponding dependence of the Ginibre distribution [96, 101, 102], one may conclude that our result is nothing more than the Ginibre distribution. As we show in Fig. 3.12, that is not true. In order to compare our distribution with the Ginibre we calcluate the corresponding distribution for a full complex matrix and compare with our result of Fig. 3.11 (black dotted line). The conclusion of such comparison, based on Fig. 3.12, is clear. The level spacing statistics of our matrix is not properly described by the Ginibre distribution, as our model's matrix is a sparse (block tridiagonal) matrix which possesses the additional symmetry: $\hat{\mathrm{H}}^{\dagger} = \hat{\mathrm{H}}^{*}$. These two features make the level spacing statistics different from the well known Ginibre distribution, which coincides

with the the full complex matrix and not with the sub-Wigner [Fig. 3.12(a)]; in contrast our distribution is clearly different from the Ginibre and coincides with the sub-Wigner [Fig. 3.12(b)].

Before closing, we would like to comment on a crucial point: is there an Anderson transition in a 2-D non-Hermitian system, or all states are localized even for very week disorder as in the Hermitian case? As we pointed out in the previous paragraphs, the presence of weak imaginary disorder, by breaking the time reversal, reduces the probability of a quantum particle to remain in the same region and hence it favors delocalization. This tendency is further supported by the level spacing exhibiting for weak disorder an s^3 dependence as s tends to zero; moreover, the increase of the extent length shown in Fig. 3.10 for weak increasing imaginary disorder provides further support to the tendency for delocalization in the presence of weak imaginary disorder. At this point we think that is difficult to definitely conclude if there is an Anderson transition in non-Hermitian 2-D case. Nevertheless, in a recent paper based on our work [103], Huang and Shklovskii reached the conclusion that the localization properties in our model are qualitatively the same as in the corresponding Hermitian model, namely that all states are localized in 2-D and that there is an Anderson transition in 3-D; this transition occurs at substantially lower critical disorder than that of the Hermitian case ($W = 6.15$ vs $W = 16.5$). The authors based their conclusion on the numerical behavior of the ratio of the second to the first nearest neighbor level spacing (see [104] for a detailed analysis of the method), both defined as in Eq. 3.17.

Chapter 4

Binary disorder

In this chapter, we will study the effects of binary disorder in 1-D tight-binding lattices, with or without short-range correlations (such as those encountered in a dimer lattice). Our study is again focused on the new phenomena that stem from non-Hermiticity.

4.1 Hermitian binary disorder

The Hermitian one-dimensional model with binary disorder with or without short range correlations has been studied intensively, both theoretically and experimentally [89, 105, 106, 107], since it is the simplest disordered system which, in spite of being one-dimensional, still facilitates wavepacket delocalization. Here we repeat some of the basic calculations regarding this model, in order to be able to compare these results with the corresponding new ones associated with its non-Hermitian generalization.

To begin with, we consider a waveguide array that exhibits a binary distribution of either ϵ_a or ϵ_b of its propagation constants, with the same probability $\mathrm{p} = \frac{1}{2}$ and without any correlations:

$$\text{Uncorrelated binary disorder}: \epsilon_n = \begin{cases} \epsilon_a, & \text{with} \quad \mathrm{p}_1 = \frac{1}{2} \\ \epsilon_b, & \text{with} \quad \mathrm{p}_2 = \frac{1}{2} \end{cases} \tag{4.1}$$

where $\epsilon_{a,b} \in \mathbb{R}$ (Hermitian case). We also assume that the coupling coefficient between neighboring channels is constant and equal to c.

To begin with we examine the evolution pattern assuming a single-channel excitation in the middle of our lattice, namely: $\psi_n(z = 0) = \delta_{n,n_0}$, where $n_0 = \kappa + 1$ (here we assume that the total site number is odd $N = 2\kappa + 1$.). More specifically, we are interested to consider the averaged variance of the

intensity pattern as a function of the propagation distance z, defined as:

$$M(z) \equiv \langle \sum_n (n - n_0)^2 |\psi_n(z)|^2 \rangle \tag{4.2}$$

where $\langle .. \rangle$ denotes averaging over many realizations of disorder.

Our numerical calculations for this case are shown in Fig. 4.2(a),(b) and are in agreement with the corresponding experimental results of [107], which are also presented as insets for direct comparison. For $\epsilon_a = \epsilon_b \Rightarrow \delta\epsilon \equiv \epsilon_a - \epsilon_b = 0$ the lattice is periodic and $M \sim z^2$, which indicates ballistic transport. If we set $\epsilon_a \neq \epsilon_b$ though, all the states become exponentially localized and $M(z)$ saturates for large values of z; we get localization in this case since $M \sim z^0$. The single-channel excitation remains localized near its initial position.

However, one gets completely different physical results if short-range order is introduced in this model. For that purpose, we now consider a "dimer" waveguide array, where each dimer consists of two subsequent channels with the same propagation constant (see schematic in Fig. 4.1); this is a model originally introduced by Dunlap. et. al. [89]:

$$\text{Dimer array} : \epsilon_{2n} = \epsilon_{2n+1} = \begin{cases} \epsilon_a & \text{with} \quad \mathrm{p}_1 = \frac{1}{2} \\ \epsilon_b & \text{with} \quad \mathrm{p}_2 = \frac{1}{2} \end{cases}. \tag{4.3}$$

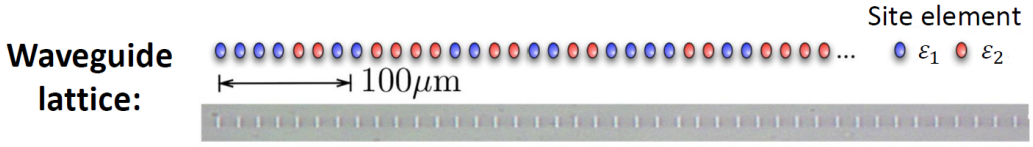

Figure 4.1: Upper row: schematic representation of the random dimer model. Bottom row: microscope image of the waveguide array used in the experiment [107].

Repeating the same calculations as in [89], we can see that now, $M \sim z^\gamma$, in all the cases, where $\gamma \simeq 2$, $\frac{3}{2}$, 1 and 0, which correspond to ballistic, superdiffusive, diffusive and localized motion, accordingly (computed numbers are: 1.99, 1.56, 0.98, 0.15) for $\frac{\delta\epsilon}{c} = 0$, 1, 2 and 3 respectively. These results indicate that the spectrum now possesses delocalized eigenvectors. Indeed, one can prove that eigenstates with eigenvalue $\omega = \epsilon_{a,b}$ are extended, as long as $|\delta\epsilon| \leq 2c$. All the relevant results are presented in Fig. 4.2(c),(d) and are again in perfect agreement with the experimental ones (insets) [107].

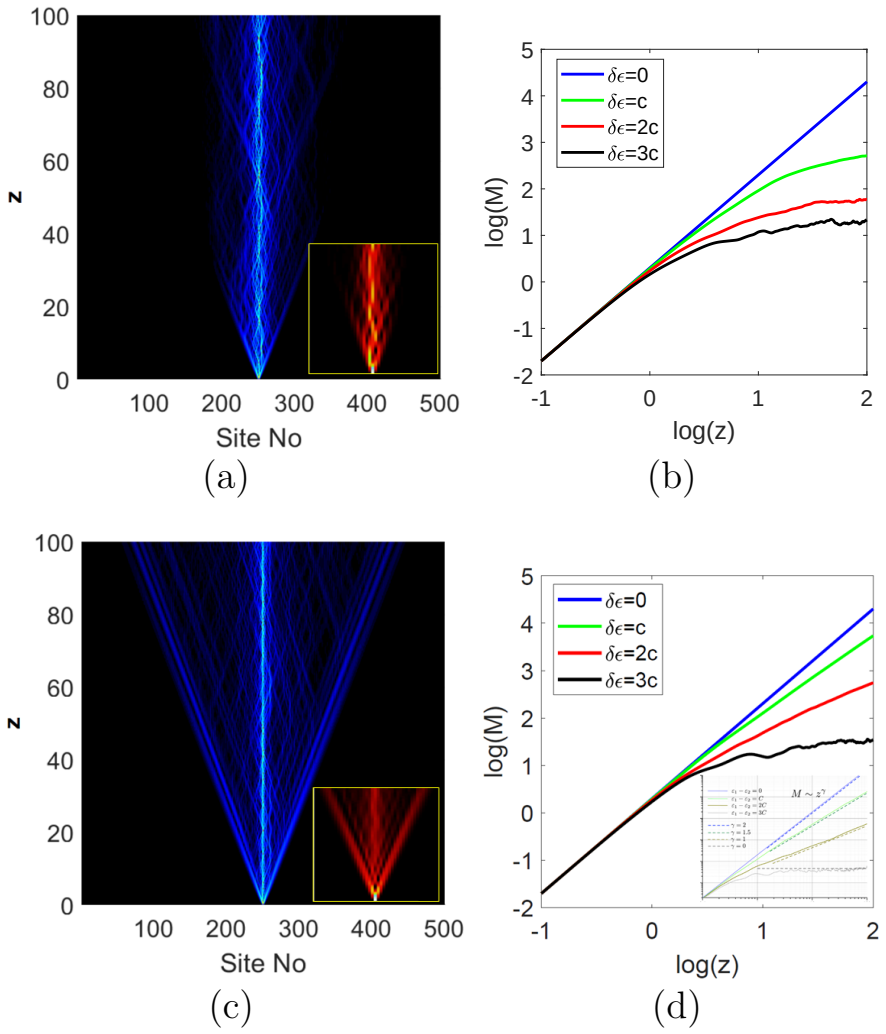

Figure 4.2: (a) Field amplitude $|\psi|$ as a function of the propagation distance z, for the uncorrelated case with $\delta\epsilon = c$. (b) Logarithm of the averaged variance M as a function of $\log z$ for the uncorrelated case and for different values of $\frac{\delta\epsilon}{c}$. (c,d) Same as in (a,b) but for the random dimer lattice (see [107]). Experimental results from [107] are also presented as insets for comparison.

A direct way to obtain a physical insight of these results is to consider a periodic lattice with a single dimer defect (see Fig. 4.3); that is:

$$\text{Dimer defect lattice:} \quad \epsilon_n = \begin{cases} \epsilon_a & \text{if} \quad n = 0, 1 \\ \epsilon_b & \text{otherwise} \ . \end{cases} \tag{4.4}$$

For $n \leq -1$ we have both an incident and a scattered wave:

Figure 4.3: Schematic representation of a lattice with a single dimer impurity.

$$\psi_n = e^{ikn} + re^{-ikn}, \quad n \leq -1 \tag{4.5}$$

while for $n \geq 1$ we have only a transmitted wave:

$$\psi_n = te^{ikn}, \quad n \geq 1 \ . \tag{4.6}$$

In this case, the tight-binding relation 2.12 for $n = -1$ reads:

$$\begin{gathered}\psi_0 = (\omega - \epsilon_a)\psi_{-1} - \psi_{-2} = (e^{ik} + e^{-ik})(e^{-ik} + re^{ik}) - e^{-2ik} - re^{2ik} \Rightarrow \\ \Rightarrow \psi_0 = 1 + r \ .\end{gathered} \tag{4.7}$$

Similarly, for $n = 1$ we get:

$$\begin{gathered}\psi_0 = (\omega - \epsilon_b)\psi_1 - \psi_2 = (e^{ik} + e^{-ik} + \delta\epsilon)te^{ik} - te^{2ik} \Rightarrow \\ \Rightarrow \psi_0 = t(1 + \delta\epsilon \cdot e^{ik}) \ .\end{gathered} \tag{4.8}$$

where

$$\delta\epsilon \equiv \epsilon_b - \epsilon_a. \tag{4.9}$$

Combining these two equations we have:

$$t = \frac{1+r}{1 + \delta\epsilon \cdot e^{ik}} \ . \tag{4.10}$$

On the other hand, the eigenvalue equation for $n = 0$ reads:

$$\begin{gathered}(\omega - \epsilon_b)\psi_0 = \psi_1 + \psi_{-1} \Rightarrow (e^{ik} + e^{-ik} + \delta\epsilon)(1 + r) = te^{ik} + e^{-ik} + re^{ik} \Rightarrow \\ \Rightarrow e^{ik} + re^{-ik} + \delta\epsilon(1 + r) = \frac{1+r}{e^{-ik} + \delta\epsilon} \Rightarrow r = \frac{-\delta\epsilon \cdot [\delta\epsilon + 2\cos(k)]}{(\delta\epsilon + e^{-ik})^2 - 1} \ .\end{gathered} \tag{4.11}$$

Thus, we obtain our final expression for the reflectance $\mathrm{R} \equiv |r|^2$:

$$\mathrm{R} = \frac{\delta\epsilon^2[\delta\epsilon + 2c\cos(k)]^2}{\delta\epsilon^2[\delta\epsilon + 2c\cos(k)]^2 + 4c^4\sin^2(k)} \ . \tag{4.12}$$

From this relation we can see that waves with $\omega = \epsilon_{a,b}$ are perfectly transmitted, provided that $|\delta\epsilon| \leq 2c$. Furthermore, it was found that the total number of states with localization length greater than the system's size is of measure $\sqrt{N}$ [89]. Thus, in Fig. 4.2(c), the two propagating peaks correspond to these $\sim \sqrt{N}$ delocalized states, leading to transport, while the

central peak indicating no propagation is associated with the vast majority of localized states.

The criterion for localization originally proposed by Anderson [3] was the asymptotic behavior of the amplitude of the wavefunction around its initial site, in the sense that absence of diffusion is associated with the limit: $\lim_{z\to\infty} |\psi_{n_0}(z)|$ being non-zero. Hence, it is reasonable to examine the probability $\Pi(z)$ for the wave to be located in its initial position as a function of the propagation distance for the two cases of disorder discussed here.

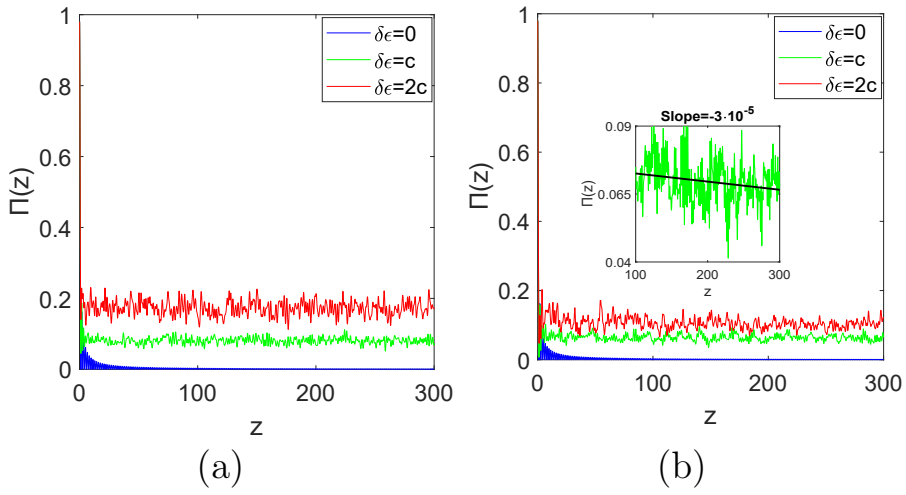

Figure 4.4: Probability $\Pi(z)$ for the wave to being found in its initial position as a function of the propagation distance z for (a) the uncorrelated binary disorder and (b) the dimer case and for different values of $\frac{\delta\epsilon}{c}$. An averaging over 50 realizations of disorder has been performed for each plot. Inset: a zoom in the plot of Π vs z for $\delta\epsilon = c$ (green line) and the least square fitting of the curve (black line). The slope of the line is shown in the title of the graph.

In Fig. 4.4 we show plots of $\Pi(z)$ for the uncorrelated binary [Fig. 4.4(a)] and the dimer array [Fig. 4.4(b)], for $\delta\epsilon/c = 0, 1$ and 2. The difference between the two graphs is small but crucial. While in Fig. 4.4(a), and for $\delta\epsilon \neq 0$, $\Pi(z)$ fluctuates around a specific, constant value, in Fig. 4.4(b) $\Pi(z)$ slowly drops as z increases, with a slope of $\sim 10^{-5}$, which is actually the value of the localization length for ω near $\epsilon_{1,2}$. This is shown clearly in the inset of Fig. 4.4(b), where a least square fit (black line) is also plotted with $\Pi(z)$. This statement is in agreement with Anderson criterion of localization, as it should be. However, due to the many fluctuations and the very small

value of the linear fitting's slope, $\Pi(z)$ is not a convenient numerical criterion for localization in this case.

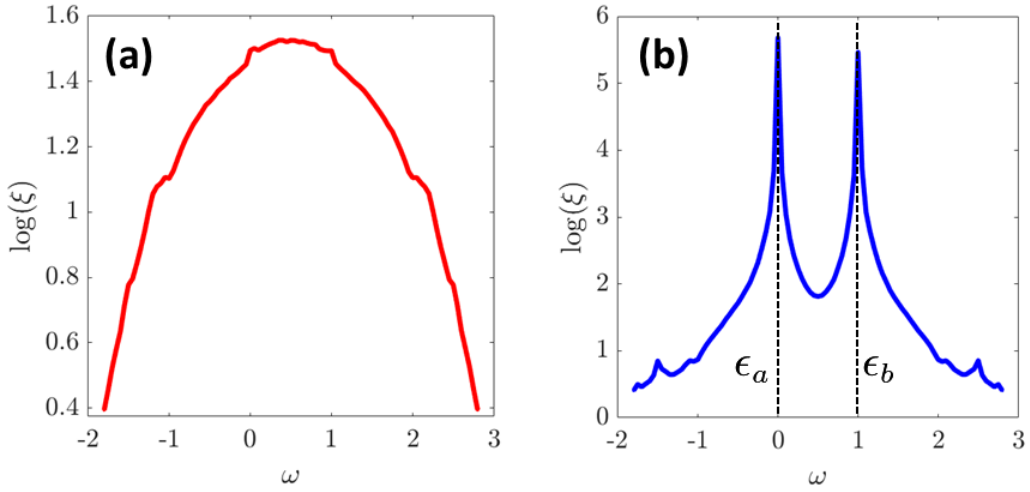

Figure 4.5: Logarithm (base 10) of localization length ξ as a function of the eigenvalue ω for (a) uncorrelated binary disorder and (b) the random dimmer model, both for $\delta\epsilon = c$.

Finally, in Fig. 4.5, we plot the localization length ξ, given by Eq. 2.19, as a function of the eigenvalue ω and for both cases of binary disorder: with [Fig. 4.5(a)] and without [Fig. 4.5(b)] short range correlations. We can clearly see that in case (a) ξ remains finite and $\ll N$, while in (b) the value of ξ diverges near $\omega = \epsilon_{a,b}$, indicating delocalization.

4.2 Non-Hermitian binary disorder

In this section we study the spectral and dynamic properties of one-dimensional waveguide lattices, which are characterized by non-Hermitian binary disorder with short range order. Our model, shown in Fig. 4.6, can be considered as the non-Hermitian extension of the random dimer model presented in the previous section. Here we show, both numerically and analytically, that in our non-Hermitian model, delocalization is impossible, for any value of the complex diagonal elements. Furthermore, we find that such a system exhibits various unexpected features, such as fractal-like spectrum, as well as regions in the complex plane where many eigenvalue come arbitrarily close and form

"eigenvalue condensates". Despite the strong Anderson localization, non-Hermitian dynamics with sudden jumps between eigenstates localized around distant sites is possible for rectangular distribution as well.

Once we consider complex propagation constants-ϵ_n, then the problem is described by a random non-Hermitian Hamiltonian. In particular, we consider initially a pair correlated (dimer) waveguide array, where each dimer consists of two subsequent channels with the same propagation constant. Each diagonal element ϵ_n is a complex random variable of a binary distribution. Initially we set $\mathrm{Re}(\epsilon_n) = 0$, while the $\mathrm{Im}(\epsilon_n)$ is a random variable from a binary pair-correlated (dimer) distribution as follows:

$$\epsilon_{2n} = \epsilon_{2n+1} = \begin{cases} i\alpha, & \text{with} \quad \mathrm{p}_1 = \frac{1}{2} \\ -i\alpha, & \text{with} \quad \mathrm{p}_2 = \frac{1}{2} \end{cases} \tag{4.13}$$

with α being a real number which describes the disorder's amplitude, and $\mathrm{p}_{1,2}$ the associated probabilities. The pair-correlation is introduced by assigning to each pair of consecutive sites the same diagonal element, which obtains two possible values of $\epsilon_{2n} = \epsilon_{2n+1} = +i\alpha$ and $\epsilon_{2n} = \epsilon_{2n+1} = -i\alpha$, with equal probabilities. A relevant schematic is represented in Fig. 4.6.

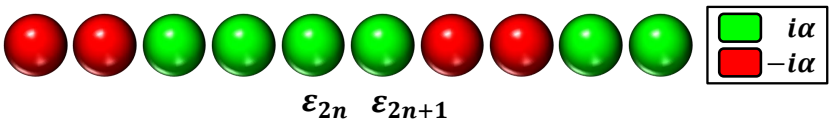

Figure 4.6: Schematic representation of the complex diagonal matrix elements for the non-Hermitian random binary pair-correlated model.

To begin with, we present plots of the system's spectrum in the complex plane for various values of the disorder's strength α, in Fig. 4.7. The spectrum for small values α is concentrated near the real axis, except for the edges whose imaginary part extends through $(-\alpha, \alpha)$ [Fig. 4.7(a)]. These results are reasonable, and can be intuitively related to the density of states of the corresponding Hermitian problem. However, for $\alpha = 0.5$ the picture is quite different. The whole spectrum now tends to move away from the real axis and to form an intricate fractal-like structure in the complex plane [Fig. 4.7(b)], which resembles the spectrum of the quasi-periodic Harper model [108], in exhibiting a similar regularity in spite of its randomness. In addition, a gap opens around the imaginary axis $\mathrm{Re}(\omega) = 0$. We have to note here that the formation of a fractal-like complex spectrum has also been reported in some other systems described by non-Hermitian random matrices [109]. Moving back to our own case, it must be pointed out that the aforementioned features

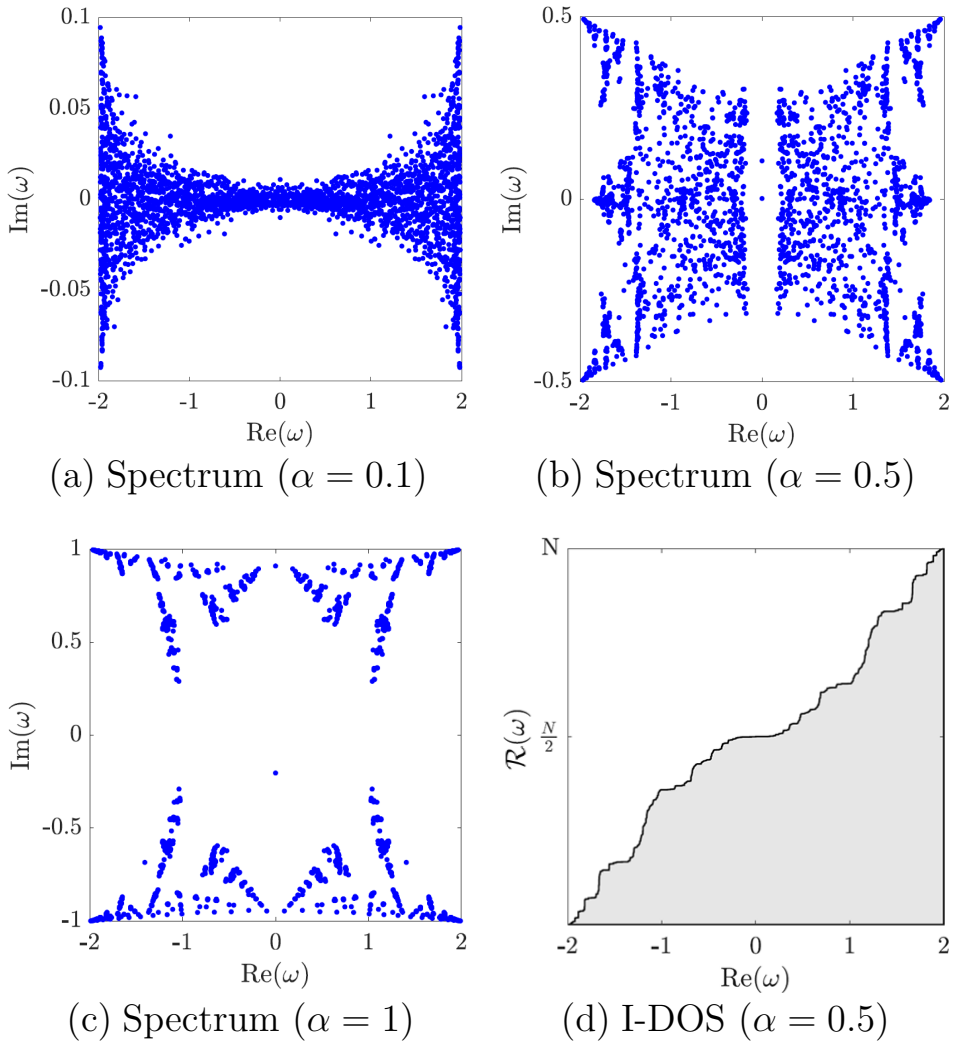

Figure 4.7: (a)-(c) Eigenvalue spectrum on the complex plane for the non-Hermitian random binary pair-correlated model and for (a) $\alpha = 0.1$, (b) $\alpha = 0.5$ and (c) $\alpha = 1$. (d) Integral density of states (I-DOS) $\mathcal{R}(\omega)$, as a function of the real part $\mathrm{Re}(\omega)$ of the eigenvalues for $\alpha = 0.5$ ($\mathcal{R}(\omega)$ counts all states with $\mathrm{Re}(\omega_j) \leq \omega$). All these results correspond to $N = 3000$.

are associated with the binary pair-correlated character of our model; they disappear in the absence of pair-correlation and in the case of a rectangular distribution of the random variable. Interestingly, if we further increase the value of α, the obtained eigenvalues do not extend over the whole complex plane, as one might expect, but they rather tend to "collapse" into specific spots [Fig. 4.7(c)], leading to a rather sparse spectrum. We term this un-

usual behavior as "eigenvalue condensation". Another way to capture this phenomenon is by plotting the integral density of states (I-DOS) $\mathcal{R}(\omega)$ as a function of the real part of the eigenvalues $\mathrm{Re}(\omega)$ [Fig. 4.7(d)]. $\mathcal{R}(\omega)$ counts all states whose eigenvalue's real part is $\leq \omega$: $\mathcal{R}(\omega) \equiv \sum_j \theta[\omega - \mathrm{Re}(\omega_j)]$, with $\theta(x)$ being the Heaviside step function. We can clearly see the step-like behavior of $\mathcal{R}(\omega)$ due to the condensation. The formed plateaus and jumps denote the absence and the coalescence of eigenvalues, respectively. If we further increase the value of α, the eigenvalues gradually approach the lines with $\mathrm{Im}(\omega) = \pm\alpha$, i.e. they tend to take the form of the diagonal matrix elements as expected, and the intriguing, yet unexplained, pattern of the spectrum is lost.

A quantification of the aforementioned change in the spectrum's picture, taking place for α between 0.1 and 0.5, is given by the level spacing distribution $\mathrm{P}(s)$, where s is the normalized minimum distance between two eigenvalues in the complex plane: $s|_{\omega_j} \equiv \min|\omega_j - \omega_{j'}|$ $(j \neq j')$. For $\alpha = 0.1$ we get the expected Wigner-Dyson distribution: $\mathrm{P}_{WD}(s) = \frac{\pi s}{2} e^{-\frac{\pi s^2}{4}}$, as seen in Fig. 4.8(a). The small deviation from this theoretical prediction we obtain is also anticipated, due to the extra symmetries governing our (effective) Hamiltonian. Nevertheless, this result implies that, for this value of α, the system is at the delocalized phase, in the sense that the mean localization length is larger than or comparable to the system's size, and its eigenvalues show level repulsion: $\mathrm{P}(s = 0) = 0$. Setting $\alpha = 0.5$ though, yields a rather unexpected level spacing distribution form [Fig. 4.8(b)]. Even though the distribution seems to exhibit a regular exponential decay for $s \gtrsim 1$, just like the classical Poisson distribution, the abrupt drop near $s = 0$ cannot be described by any exponential function. Moreover, the (computed) values of $\mathrm{P}(s)$ in this region appear to have an almost inversely proportional dependence on the value of the averaging interval Δs (bar's width in Fig. 4.8(b)). These observations lead us to the conclusion that the level spacing distribution possesses a singularity for $s = 0$; in particular, we estimate that $\mathrm{P}(s)$ diverges as $s^{-\beta}$ $(\beta > 0)$ for $s \to 0$, and thus it can be approximated by the following expression:

$$\mathrm{P}_F(s) = A s^{-\beta} e^{-\lambda s} \ . \tag{4.14}$$

In Fig. 4.8(b), a curve fitting in the form of $\mathrm{P}_F(s)$ is also plotted (red line) together with $\mathrm{P}(s)$, showing that such a function can describe the basic characteristics of the level spacing distribution with a satisfactory precision. We also think that the singular behavior for $s \to 0$ is in agreement with the aforementioned eigenvalue condensation, since a large number of eigenvalues tend to come arbitrary close to each other.

The next important issue we would like to address, is whether or not delo-

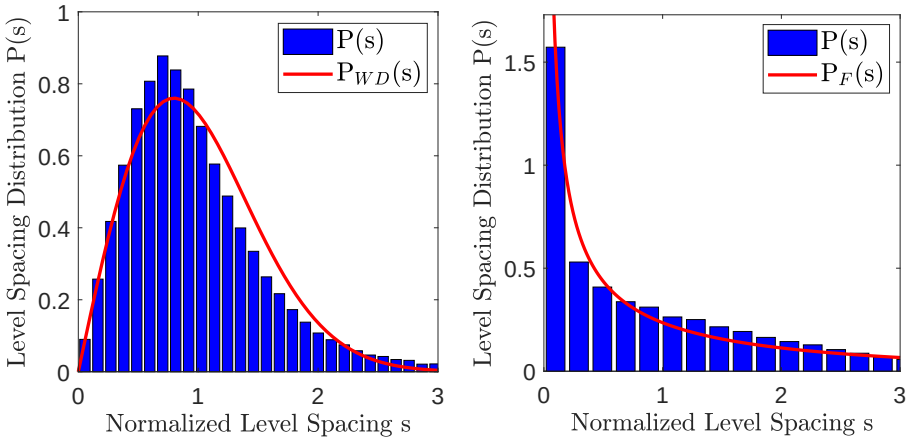

Figure 4.8: Normalized level spacing distribution P(s), averaged over the whole spectrum, for (a) $\alpha = 0.1$, compared to the Wigner-Dyson distribution (red curve), and (b) $\alpha = 0.5$, fitted with a function of the form of Eq. 4.14 (red curve), with: $A \approxeq 0.3$, $\beta \approxeq 0.72$ and $\lambda \approxeq 0.24$. An averaging over 50 realizations of disordered systems with $N = 2500$ has been performed for these results.

calization in this non-Hermitian model is possible. A direct and elegant way to see this is by considering the scattering amplitude from a non-Hermitian dimmer impurity, as we did in the previous section (see Eq. 4.11). For the non-Hermitian dimer, the expression reads:

$$\mathrm{R} = \frac{\alpha^2(\cos^2 k + \alpha^2)}{(1 + 2\alpha^2 - 2\alpha \sin k)^2 - \cos^2 k} \ . \tag{4.15}$$

The above relation clearly shows that the equation R = 0 does not admit acceptable solutions as long as the on-site energies become imaginary, indicating that, contrary to the Hermitian case, all the eigenstates are now localized.

In order to verify this statement, we need to calculate the localization length ξ, defined in Eq. 2.19. Note that, in practice, if N is much larger than ξ (which in our case holds true since $N/\xi > 50$), one obtains a reliable value of ξ as $n \to N$. A plot of ξ as a function of the value of ω on the complex plane is shown in Fig. 4.9. We can clearly see that our assessment of complete localization was correct, since N/ξ does exceed the value of 50. Moreover, we find that ξ remains finite for every value of $\alpha \neq 0$. The fact that all eigestates of the spectrum are localized, in contrast to the Hermitian

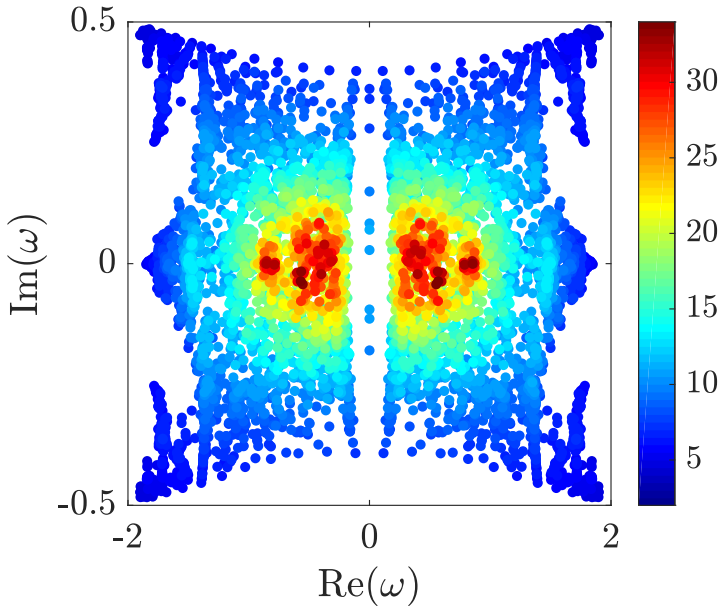

Figure 4.9: Localization length ξ (colorbar) of the eigenstates for the non-Hermitian random pair-correlated lattice, as a function of the corresponding eigenvalue ω on the complex plane and for $\alpha = 0.5$. We can see that the localization length does not exceed the value of 35 (N = 2000, 5 realizations of disorder are superimposed for visualization purposes).

case, is one of the most direct consequences of the non-Hermiticity on our system.

So far we have investigated the spectral properties of our model. However, dynamic phenomena associated with the spreading of an initially local excitation are the most intriguing and unexpected ones. In order to systematically study the wave dynamics, we examine the evolution pattern and the variance M(z) (notice that M(z) corresponds to only 1 realization, while $M(z)$ represents the average variance) of an initial single-channel excitation as a function of z. Once again, the single channel was chosen to be at the center of the lattice; thus, $\psi_n(z = 0) = \delta_{n,n_0}$, where n_0 is the index of the middle channel of the lattice.

For $\alpha = 0$ the lattice is periodic and M$\sim z^2$, as expected, which is a characteristic of ballistic transport. If we set $\alpha \neq 0$, although all states become exponentially localized, M(z) exhibits a very interesting behavior. Our results are depicted in Fig. 4.10. Note that, in order to obtain the desired physical picture, we have plotted the power-normalized field amplitude: $|\phi_n| = \frac{|\psi_n|}{\sqrt{\mathcal{P}(z)}}$, where the denominator $\mathcal{P}(z) \equiv \sum_n |\psi_n|^2$, describing the total

field power, is used to force energy conservation, since the field amplitude $|\psi_n|$ diverges exponentially as $z \to \infty$, due to the presence of gain.

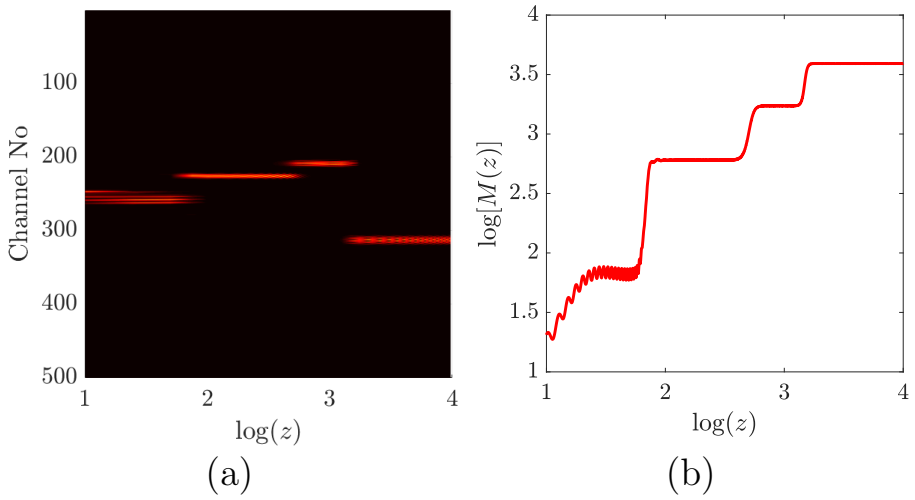

Figure 4.10: (a) Normalized field amplitude $|\psi_n|$ as a function of the propagation distance's logarithm $\log z$. (b) Logarithm of the variance M as a function of $\log z$. For these results we have set $\alpha = 1$ and N=501.

The wave evolution pattern is rather surprising. Even though all the eigenstates are localized, the wave exhibits "non-Hermitian jumps" between distant sites and thus we obtain energy spreading which seems to continue until the edges of the system are reached. This behavior is also captured by the plot of the variance over z in Fig. 4.10(b), for the same realization of disorder, which also exhibits a number of finite jumps. This behavior occurs only in non-Hermitian systems and has not a Hermitian analogue. In order to understand the physical mechanism behind this unexpected feature, we calculate the field at $z = z_{max} = 10^4$ for the same realization of disorder as in Fig. 4.10(a), and compare it with the field profile of the most gainy mode, namely the mode which corresponds to the eigenvalue with the largest value of the real part of $i\omega$, in Fig. 4.11(d).

In trying to physically interpret these intriguing results we have to stress two features of the eigenstates (left or right) which are unique in disordered random non-Hermitian systems: (a) their complex eigenvalues ω_j which lead to either infinite or zero amplitude as $z \to \infty$ depending on the sign of $\mathrm{Im}(\omega_j)$, (b) their non-orthogonality which facilitates transfer of energy from channel to channel, even between distant channels. These two features seem to account for the jumpy spread of energy; indeed, as we have pointed out before, a gainy mode, i.e. one combining a large negative value of $\mathrm{Im}(\omega_j)$,with

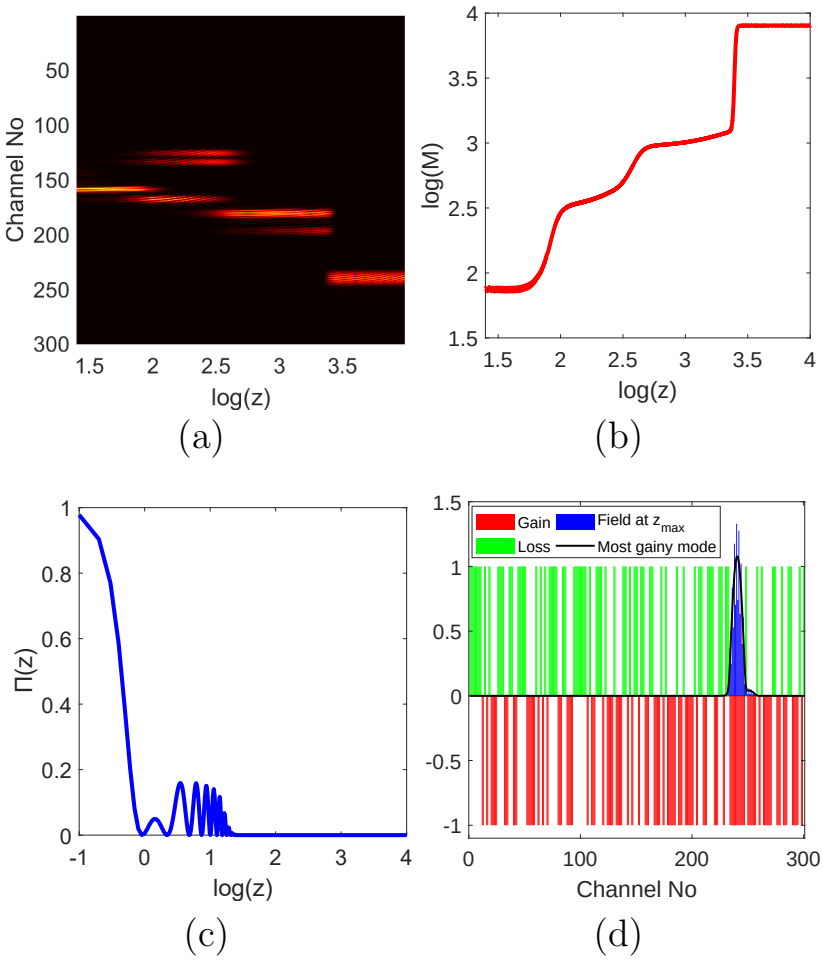

Figure 4.11: (a) $|\psi_n|$ as a function of $\log z$, under a particular realization with $\alpha = 1$. (b) Logarithm of the variance M as a function of $\log z$. (c) Probability Π for the wave to return to its initial position as a function of z. (d) $|\psi_n|$ near the end of the lattice $z = z_{max}$ (blue bars). The field profile of the most gainy eigenstate is also plotted here for comparison (black line). The gain and loss distributions (imaginary part of the potential) are depicted with red, green color, respectively. In all the above, $N = 301$.

a large overlap with the initial (or any intermediate) state is in a privileged situation (compared with a next neighboring channel) to be the recipient of an excitation. We have confirmed this behavior by several numerical experiments in which we artificially introduced states with a large negative $\mathrm{Im}(\omega_j)$ and located at selected sites. Always the jumps occur at these sites even when they were far away from the initial site. Can we conclude from these

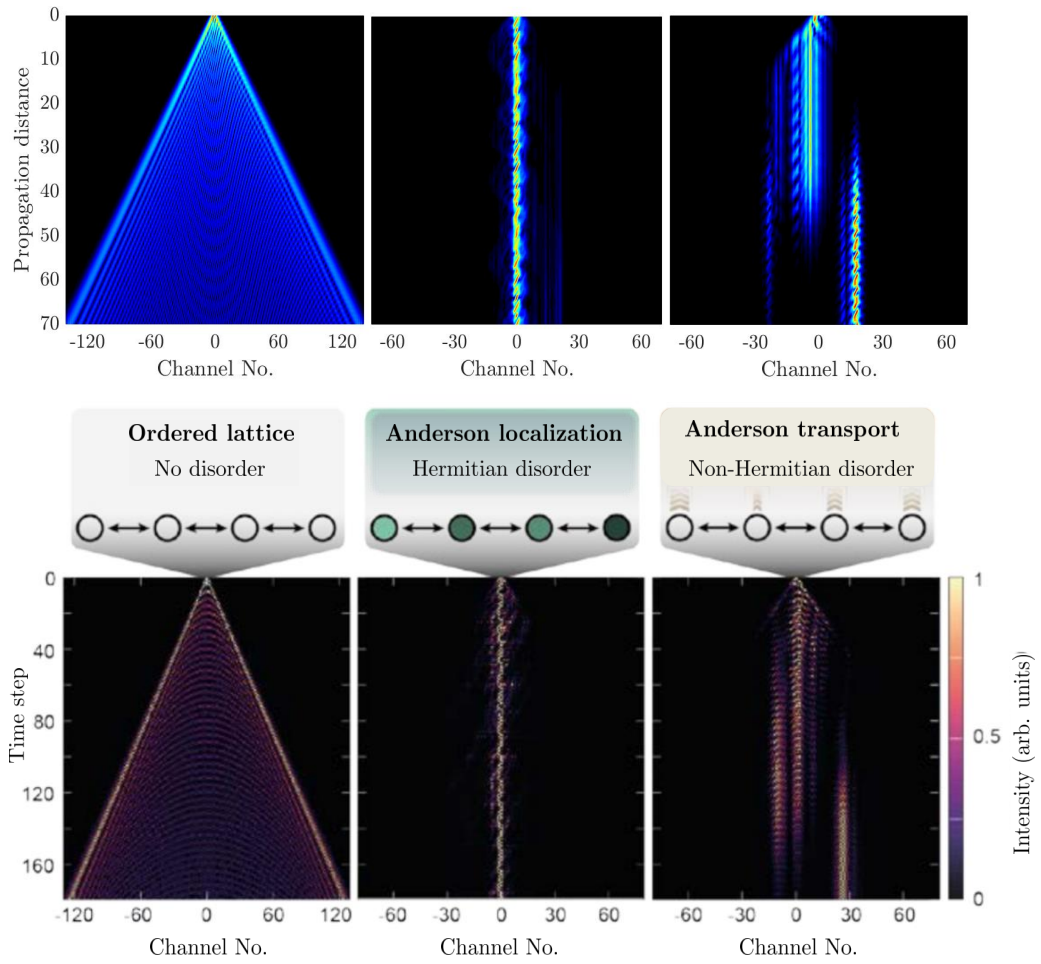

Figure 4.12: Comparison between our theoretical/numerical results (upper row) and the corresponding experimental ones from [110]. Propagation through a waveguide lattice shows ballistic spreading for homogeneous lattices (left) compared to Anderson localization in Hermitian disordered lattice (center) and the jumping between localized states in the case of a non-Hermitian disordered lattice (right).

results that disordered random non-Hermitian systems with a short localization length allows a new type of transport by jumps to privileged eigenstates? The answer is not necessarily yes. The reason is that one has to be careful when referring to transport for non-Hermitian systems, because there are no intrinsic conservation laws. Our model being an open one, allows for offering (gain)/removing (loss) of energy to/from our system in addition of transporting the energy initially excited at a single site. It seems difficult or even

impossible to distinguish between these two different physical mechanisms. Nevertheless, by examining the z-evolution of an initially local state in connection with the behavior of the total power $\mathcal{P}(z)$ of the system as a function of z, we found that the problem under question goes well beyond the amplification explanation and that transport by jumps occur even in the purely dissipative case. Thus, for the case of externally forced energy conservation and small z no jumps were observed, although they appear for large enough z. Jumpy spread of the initial excitation was also found in the cases where either only loss (no gain) was imposed or normalization was replaced by gain saturation (as is usual experimentally). Thus, taking into account our own results and experimental [110] (also see Fig. 4.12 for a comparison) and other work [111, 112] we suppose that the phenomenon of unusual jumpy transport can generally occur in Anderson-localized random non-Hermitian systems, as a composite effect of gainy modes and their non-orthogonality. Finally, we note that our model seems to lack special non-Hermitian degeneracies, such as the so called exceptional points, even if the randomness is chosen to be spatially antisymmetric ($\mathcal{PT}$ symmetric case).

Chapter 5

Constant intensity waves

As mentioned in the introduction, it was recently demonstrated that is possible to suppress the effects of localization and achieve perfect transmission by considering correlated non-Hermitian disorder in photonic media. In this chapter we derive a novel class of waves that have constant intensity (CI-waves) everywhere in space, even inside the scattering area [90, 91]. Such waves exist in guided and scattering media with gain and loss in both one and two spatial dimensions [113, 114, 115]. It was also experimentally demonstrated that CI-pressure waves are possible in the acoustical domain [116]. The existing works focus on excitation of CI-waves by plane waves and so far there is no experimental observation in the optical domain. Therefore, in this work we will go beyond CI-waves (that have infinite extent) and will show that it is also possible to obtain reflectionless wavepackets that propagate through disordered environments in a similar fashion. More specifically, we will derive the correlated non-Hermitian disorder that is crucial for finite beams to be perfectly transmitted. The physical system that we are going to investigate is that of coupled paraxial waveguide arrays. Both disorder and gain/loss can be implemented in this type of versatile integrated platform, which is ideal for controlled optical experiments. Diagonal, as well as off-diagonal disorder, in the complex refractive index and the coupling coefficients respectively, will be systematically examined in 1+1 dimensional lattices. The robustness of such an effect and the relations of these wavepackets to CI-waves will be studied in detail.

5.1 Continuous limit and CI-Waves

Before we continue to the main part of our work, it is beneficial to examine the continuous limit of our discrete problem and the connection of Eq. 2.5 to CI-waves. This investigation is going to provide us with the necessary intuition for the form of the correlated non-Hermitian disorder we have to use. For this purpose we first examine the case of diagonal disorder, which means that disorder exists only on the waveguide channel, where ϵ_j takes on spatially correlated random values to make the continuum limit meaningful. By applying the gauge transformation $\psi_j = \Phi_j e^{i2cz}$ and allowing $c = \frac{1}{(\Delta x)^2}$ (see [91] for more details), the above equation in the continuum limit ($\Delta x \to 0$) can be written as:

$$i\Phi_z + \Phi_{xx} + V(x)\Phi = 0 \tag{5.1}$$

where $V(x)$ is the disordered potential. If in the above Schrödinger-type equation, that describes wave propagation in the paraxial limit, we also assume that we have a plane wave with propagation constant k_z along the z-direction: $\Phi = u(x)e^{ik_z z}$, the equation we obtain is mathematically equivalent to the 1-D Helmholtz equation.

It has been shown [90] that this equation supports constant intensity solutions, if the potential satisfies the following relation:

$$V(x) = [k_x \mathcal{W}(x)]^2 - ik_x \mathcal{W}'(x) + k_z \tag{5.2}$$

where $\mathcal{W}$ is an arbitrarily chosen real, smooth function of x and $\mathcal{W}' \equiv \frac{d\mathcal{W}}{dx}$. In the context of integrability soliton theory these potentials naturally appear and are sometimes called Wadati potentials[117, 118, 119, 120]. In the case of Eq. 5.2 with x a continuous variable, the second order Helmholtz operator $\hat{H}_e$ can be factorized [119] as follows:

$$\hat{H}_e \equiv -\hat{D}_i^2, \quad \text{where} \quad \hat{D}_i = -i\sigma_x \partial_x + \sigma_y \kappa - i\sigma_z k_x \mathcal{W}(x) \tag{5.3}$$

with $\hat{D}_i$ being the (first order) Dirac operator of the generalized Haldane model with imaginary mass, $\sigma_x, \sigma_y, \sigma_z$ are the usual Pauli matrices and $\kappa \equiv \sqrt{k_z}$. In the above expression the Pauli matrices act on the spinor $\begin{pmatrix} \mathcal{E}_1 \\ \mathcal{E}_2 \end{pmatrix}$, where $\mathcal{E}_1$ is the real and $\mathcal{E}_2$ the imaginary part of the total field: $\mathcal{E} \equiv \mathcal{E}_1 + i\mathcal{E}_2$.

One can easily verify (see [119] for details) that $\hat{D}_i$ possesses a constant intensity eigenstate[90, 91]:

$$\Phi(x, z) = \exp[ik_z z + ik_x \int_0^x \mathcal{W}(x')dx'] \tag{5.4}$$

as long as the so-called degree [121] of $\mathcal{W}$ is zero (i.e. $\mathcal{W}$ has the same sign at $\pm\infty$).

5.2 Discrete CI-Waves and Wadati wavepackets: (a) Diagonal disorder

Inspired by the previous paragraph, we will now extend our study to the discrete case, by considering the realistic physical model of Fig. 5.1. Let us assume that instead of an incoming plane wave (continuous case) we have a Bloch wave that propagates from the left sublattice ($j < 1$) of the form:

$$\psi_j(z) = \exp(ik_z z + ik_x \cdot j) \tag{5.5}$$

where k_x is the Bloch momentum that takes values inside the first Brillouin zone, namely $-\pi \leq k_x < \pi$. The propagation constant k_z in the two periodic sublattices, is directly related to the Bloch momentum k_x through the dispersion relation $k_z = 2c \cdot \cos(k_x)$, which defines the band of the lattice (in this section we assume that $c_j = c = 1$ for simplicity). On the other hand, discretization of Eq. 5.4 leads us to the following ansatz for the ψ_j, which constitutes a discrete CI-wave:

$$\psi_j(z) = \exp(ik_z z + ik_x \sum_{m=1}^{j} \mathcal{W}_m) \ . \tag{5.6}$$

Direct substitution of this ansatz into Eq. 2.5 leads us to the conclusion that we must consider a non-Hermitian potential, with a real part of the following form:

$$\epsilon_{R,j} = 2\cos(k_x) - \cos(k_x \mathcal{W}_j) - \cos(k_x \mathcal{W}_{j+1}) \tag{5.7}$$

and a corresponding imaginary part:

$$\epsilon_{I,j} = \sin(k_x \mathcal{W}_j) - \sin(k_x \mathcal{W}_{j+1}) \ . \tag{5.8}$$

From Eq. 5.7, we can see that the potential becomes periodic if $\mathcal{W}_j = 1$, $\forall j$. If $\mathcal{W}_j$ is random, then the potential takes on also random values around $2\cos(k_x)$. The strength of disorder can be controlled by adjusting the amplitude of $\mathcal{W}_j$.

Another important point is the boundary conditions on the two interfaces of the disordered region at $j = 1$ and at $j = M$ (see Fig. 5.1). In order to achieve a smooth transition from one sublattice to another, the continuity of the k_z-component across the interface is essential. Thus, we need to apply the appropriate boundary conditions for the function $\mathcal{W}$, which are the following perfect transmission boundary conditions [113]:

$$\mathcal{W}_1 = \mathcal{W}_M = 1 \ . \tag{5.9}$$

We also need to emphasize that the above boundary conditions ensure both that the degree of $\mathcal{W}$ is zero [119, 121] and that the average of gain and loss is zero, $\sum_{j=1}^{M} \epsilon_{I,j} = 0$ (mean reality condition[113]).

The purpose of our analysis is to extend the concept of CI wave, which refers to infinite plane (or Bloch) waves, to wavepacket propagation problems, which are physically more realistic.

For the physical system we study in this chapter, we consider a total lattice that consists of three different sublattices, two periodic ones in the asymptotic regions and a disordered one in the middle. More specifically, for $j < 1$ and $j > M$ we assume two semi-infinite periodic sublattices, namely:

$$\epsilon_j = 0, \quad c_j = 1 \quad \text{for} \quad j < 1 \quad \text{or} \quad j > M \tag{5.10}$$

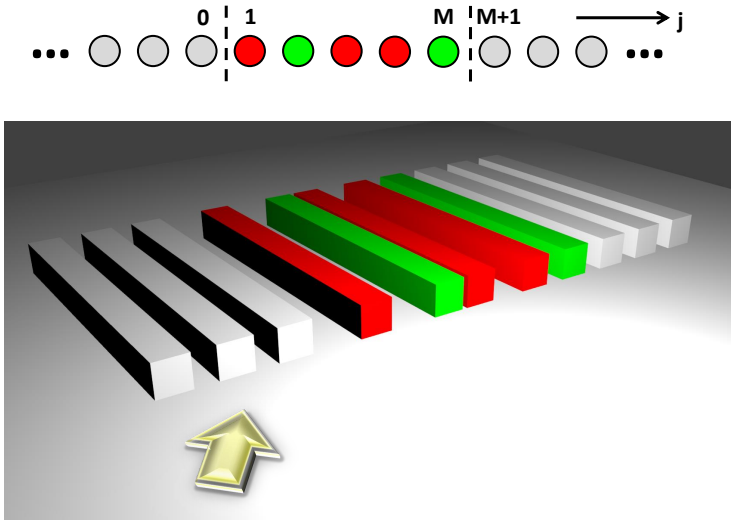

Figure 5.1: Schematic depiction of disordered waveguide structure. The two semi-infinite sublattices on the right and left are shown as gray channels. The disordered lattice on the middle ($1 \leq j \leq M$) is illustrated by red and green colored channels for gainy and lossy waveguides, respectively. The random position of the waveguides is due to the random couplings between nearest neighbors. The arrow denotes the direction of the incident Gaussian wavepacket coupled to the left periodic array.

In the middle region, $1 \leq j \leq M$, our lattice is disordered. The geometry of the problem is graphically depicted in the schematic of Fig. 5.1. In particular, we examine two different types of disorder: (a) on-site (diagonal) disorder and (b) off-diagonal disorder on the coupling coefficients.

The main focus of our study is to examine if it is possible to suppress the transverse reflection by considering complex correlated disorder. More specifically, we are interested in understanding the effect of non-Hermiticity on the transport of a finite wavepacket across the disordered region. When we have Hermitian disorder only (ϵ_j real) then most of the light is reflected in the transverse direction of the lattice and the propagation of the beam gets distorted. The question we will try to solve is whether the addition of gain and loss in form of an imaginary part of the diagonal elements ϵ_j can remedy these detrimental effects altogether. Our strategy is based on the concept of discrete CI-waves that was described in the previous paragraph. However, in the present work and for the sake of being realistic we are employing a Gaussian beam in space (or, equivalently a Gaussian wavepacket in time) instead of a pure Bloch wave. This beam/wavepacket has a central wavenumber corresponding to the discrete CI-wave and propagates from the left to the right, starting from the left periodic sublattice. The width of such a beam is denoted with σ, and its center is located around some waveguide with index $j_0 < 1$ and has a specific group velocity. As σ tends to infinity the pure Bloch wave is recaptured. In other words our initial beam can be expressed as:

$$\psi_j(z=0) = \exp[ik_x(j-j_0) - (\frac{j-j_0}{\sigma})^2] \tag{5.11}$$

Inside the disordered region, we seek finite, constant-width propagating wavepackets of the (approximate) form:

$$|\psi_j(z)| = \exp\{-[\frac{j-j_0(z)}{\sigma}]^2\}, \quad \text{with} \quad j_0(z) = j_0 + 2\sin(k_x)z \ . \tag{5.12}$$

Since these type of beams exist only for the discrete version of non-Hermitian Wadati potentials, we call these solutions "Wadati wavepackets".

Let us now examine propagation of beams through Wadati potentials (Fig. 5.2). We initially consider the Gaussian beam of Eq. 5.11 impinging on a random Hermitian potential ϵ_R of Eq. 5.7 [Fig. 5.2(a)] and then include the appropriate imaginary part based on Eq. 5.8 [Fig. 5.2(b)]. In Fig. 5.2(c),(d) the corresponding real and imaginary parts of the potential are depicted, satisfying the above smoothness condition

As one can see, in the Hermitian case the reflection due to disorder is very strong leading to very low transmission. On the contrary, for the non-Hermitian case the transmission is almost perfect and the Wadati beam/ wavepacket maintains its transverse form for every value of the propagation distance. Thus by adding the appropriate imaginary part to the real (random) potential, the beam penetrates the disordered region and propagates

with (almost) constant peak amplitude. As expected for a finite Gaussian wavepacket, it also spreads in its width during propagation.

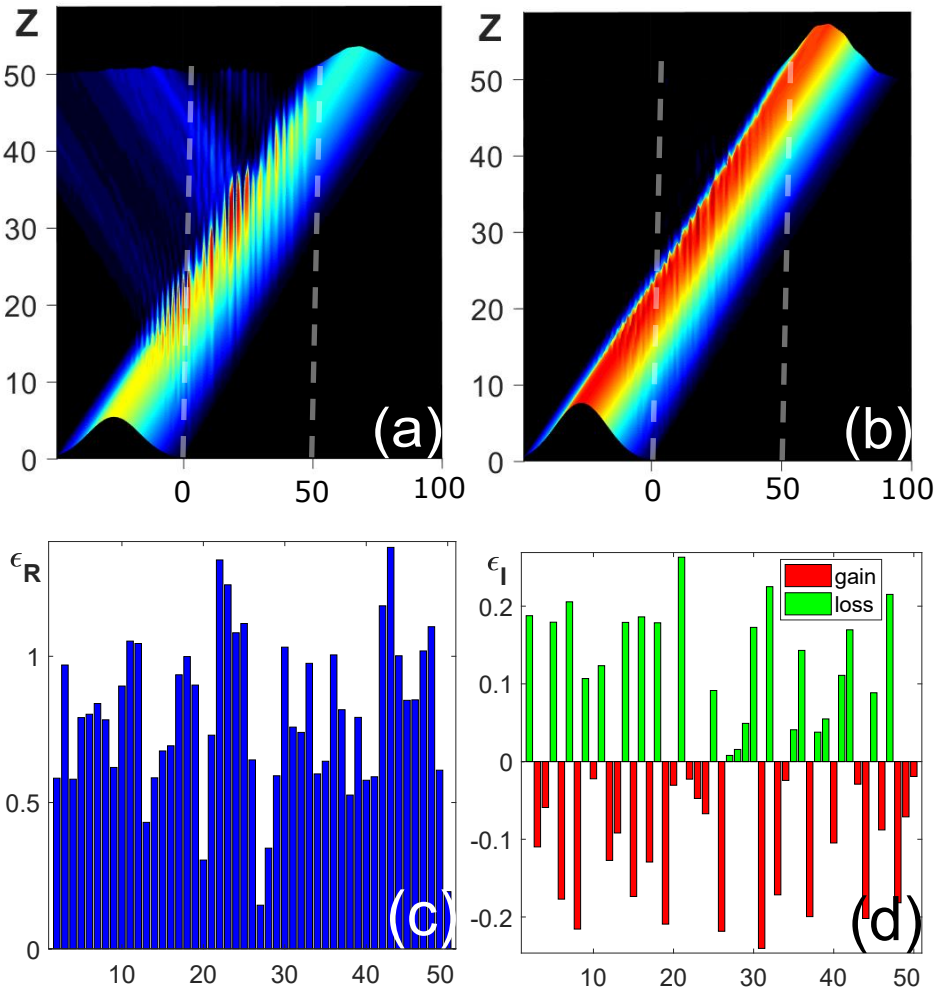

Figure 5.2: (a) Intensity of a beam propagating in a potential with real disorder (reflection occurs). (b) Same as in (a) but with imaginary part based on relation (5.8) (reflection is minimized). Dashed lines denote the interfaces among the sublattices. (c) Real part of the potential. (d) The corresponding imaginary part. In all the figures above, the x-axis represents the waveguide number j. Here we have set: $M = 50$, $j_0 = -37.5$ and $\sigma = 30$.

The price we pay for considering a Gaussian beam as our initial condition is an extra limitation. In particular, the whole analysis of the constant intensity waves (Eqs. 5.3) is based on an incident plane wave (or Bloch wave in our case) which corresponds to σ equal to infinity instead of the finite σ of our

Gaussian beam. In other words, the potential we have introduced is designed for a single wavenumber k_x while our beam is composed of a large number of different wavenumbers. The components of the beam which correspond to $k'_x \neq k_x$ will then be scattered due to the randomness of the potential and distort the pattern of the wavepacket. This effect will be sharpened if we increase the amount of the potential's randomness. As a result, in order for this distortion to be weak enough for our solution to be of the expected form, W cannot be a totally random function, but a "slowly" varying one. In other words, the jumps from one site to another should not be arbitrarily large, but rather satisfy: $\Delta\mathcal{W}_j = |\mathcal{W}_{j+1} - \mathcal{W}_j| \sim$ lattice constant $<< \sigma$, $\forall j$. Of course, in the limit of large σ, this limitation ceases, as our incident beam now becomes a Bloch wave.

We accentuate here that this shape-preserving perfect transmission of the Wadati wavepacket is unidirectional. This means that an incident beam from the right sublattice (with $k'_x = \pi + k_x$) does not lead us the same results, since the time-reversal symmetry of the lattice is broken (due to non-Hermiticity). The transmittance from the right incidence is again one, as our system is reciprocal, but we also get strong reflection. In order to get the same shape-preserving transmission from the right, we would have conjugate potential $\epsilon_j \to \epsilon_j^*$ when injecting from the opposite side.

As we have mentioned before, the non-Hermitian potential is by default designed to support a discrete CI-wave at a single transverse wavenumber k_x. Therefore an important question is how sensitive is the transmission of the corresponding Wadati wavepacket to changes of its central wavenumber. For this reason, we calculate the power ($\mathcal{P} \equiv \sum_j |\psi_j|^2$) transmitted to the right sublattice $\mathcal{P}_T$, as well as the corresponding reflected power $\mathcal{P}_R$, over the power of the input beam, after the passing of the beam through the disordered region:

$$\mathcal{P}_T \equiv \frac{\mathcal{P}_{Transmitted}}{\mathcal{P}_{Incident}} = \frac{\sum_{j=M+1}^{\infty} |\psi_j|^2}{\mathcal{P}_{Incident}} \tag{5.13}$$

$$\mathcal{P}_R \equiv \frac{\mathcal{P}_{Reflected}}{\mathcal{P}_{Incident}} = \frac{\sum_{j=-\infty}^{M} |\psi_j|^2}{\mathcal{P}_{Incident}} \tag{5.14}$$

as a function of the percentage deviation $\Delta k\%$ between the required wavenumber k_x and the beam's wavenumber k'_x: $\Delta k \equiv k'_x - k_x$. The results are shown in Fig. 5.3 and are averaged over 500 realizations of disorder. Both $\mathcal{P}_T$ and $\mathcal{P}_R$ exhibit a parabolic behavior, with the peak (dip) located at the expected value of $\Delta k = 0$. In addition, we have to note that we get $\mathcal{P}_T \simeq 1$ for a wavenumber variation $|\Delta k| \leq 10\%$; a result very close to the corresponding one from the continuous case [113].

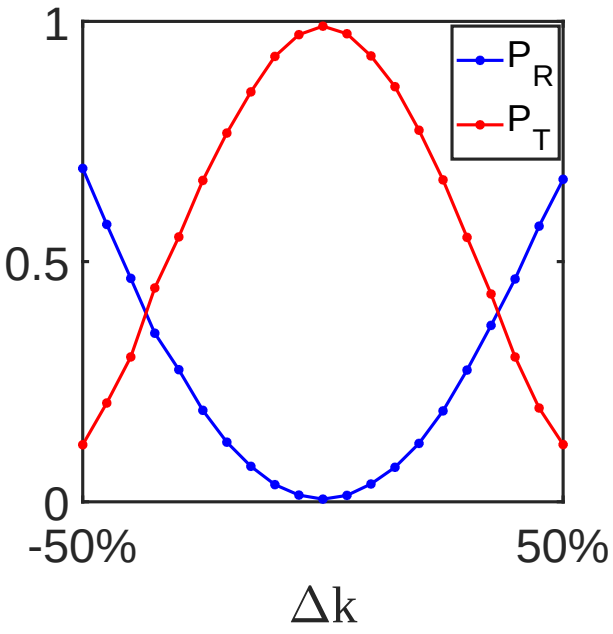

Figure 5.3: Power of the transmitted ($\mathcal{P}_T$, red line) and reflected ($\mathcal{P}_R$, blue line) wave, divided by the power of the initial beam, (Eq. 5.14), as a function of the percentage deviation (detuning) from the required wavelength value k_x: $\Delta k = k'_x - k_x$. In this case we have set $k_x = \frac{\pi}{2}$, for the case of diagonal disorder. An averaging over 500 realizations of disorder has been performed for these results.

In order to have a better physical perspective of our problem, we provide here some indicative order of magnitude estimation of the actual scales for a possible experiment. In particular, the wavelength of the beam is $\lambda_0 \approx 1\mu m$, the distance between neighboring waveguides is $D \approx 10\mu m$, while the propagation distance z is normalized over $2k_0 n_0 D^2$, with $n_0 \approx 3.5$ being the background refractive index of the waveguides and $k_0 = \frac{2\pi}{\lambda_0}$. Finally, the corresponding continuous potential is $2k_0^2 n_0 D^2(\Delta n_R + i\Delta n_I)$, where Δn represents the variation of the waveguide's refractive index with respect to the background value of n_0. Under these conditions, the maximum variation in the real part of the index of refraction is approximately $\Delta n_R^{max} \approx 10^{-3}$ and the maximum gain (loss) used is $g_{max} \approx 30 cm^{-1}$.

5.3 Discrete CI-Waves and Wadati wavepackets: (b) Off diagonal disorder

In this section we will examine whether it is possible to obtain a perfectly transmitting wavepacket for the case of random real couplings c_j, as encountered when the distance between neighboring waveguides is not the same. Since for this problem the discrete Wadati potential of the previous paragraph does not provide a straightforward solution, a new approach is required.

Substituting the ansatz of Eq. 5.6 in Eq. 2.5 once again, with the coupling coefficients c_j being random this time, the obtained potential reads as follows:

$$\begin{aligned} \epsilon_{R,j} &= 2\cos(k_x) - \cos(k_x)(c_j + c_{j-1}) \\ \epsilon_{I,j} &= \sin(k_x)(c_j - c_{j-1}) \end{aligned} \tag{5.15}$$

Our result implies that, in order to cope with the randomness in the coupling matrix elements c_j, we also need to introduce complex randomness in the potential. The potential given by the relations (5.7) and (5.8) is then modified as follows: while we need to set $\mathcal{W}_j = 1$, a factor involving the c_j must be incorporated in the $\cos(k_x)$ and $\sin(k_x)$ terms of ϵ_R and ϵ_I respectively.

The propagation of a Gaussian beam across this discrete non-Hermitian potential landscape is depicted in Fig. 5.4. In particular, we see in Fig. 5.4(a) that the strong reflection due to disorder leads to almost zero transmission. By considering the appropriate (complex) refractive index modulation the transmission becomes perfect and shape-preserving, with almost zero reflection, as is demonstrated in Fig. 5.4(b) for one particular realization of disorder.

The coupling coefficient distribution, as well as the corresponding complex potential, are also shown in Fig. 5.4. We point out here, that this case of off-diagonal disorder seems to be more robust than the case of diagonal disorder, meaning that the reflection is even more insignificant than in the results shown in Fig. 5.2.

Finally, in Fig. 5.5 we plot the transmitted and reflected power, defined by Eqs. (5.13,5.14), as a function of the wavelength detuning: $\Delta k = k_x' - k_x$. As in Fig. 5.3, $\mathcal{P}_R$ and $\mathcal{P}_T$ exhibit again a parabolic behavior. However, here the perfect transmission peak is broadened: $\mathcal{P}_T \simeq 1$ and $\mathcal{P}_R \simeq 0$ for $|\Delta k| \leq 20\%$. In addition, the reflected power, contrary to the diagonal disorder case, reaches values up to 0.3. We attribute this behavior to the trapping of the beam in lossy regions of the lattice, leading to a rapid decay in the beam's intensity.

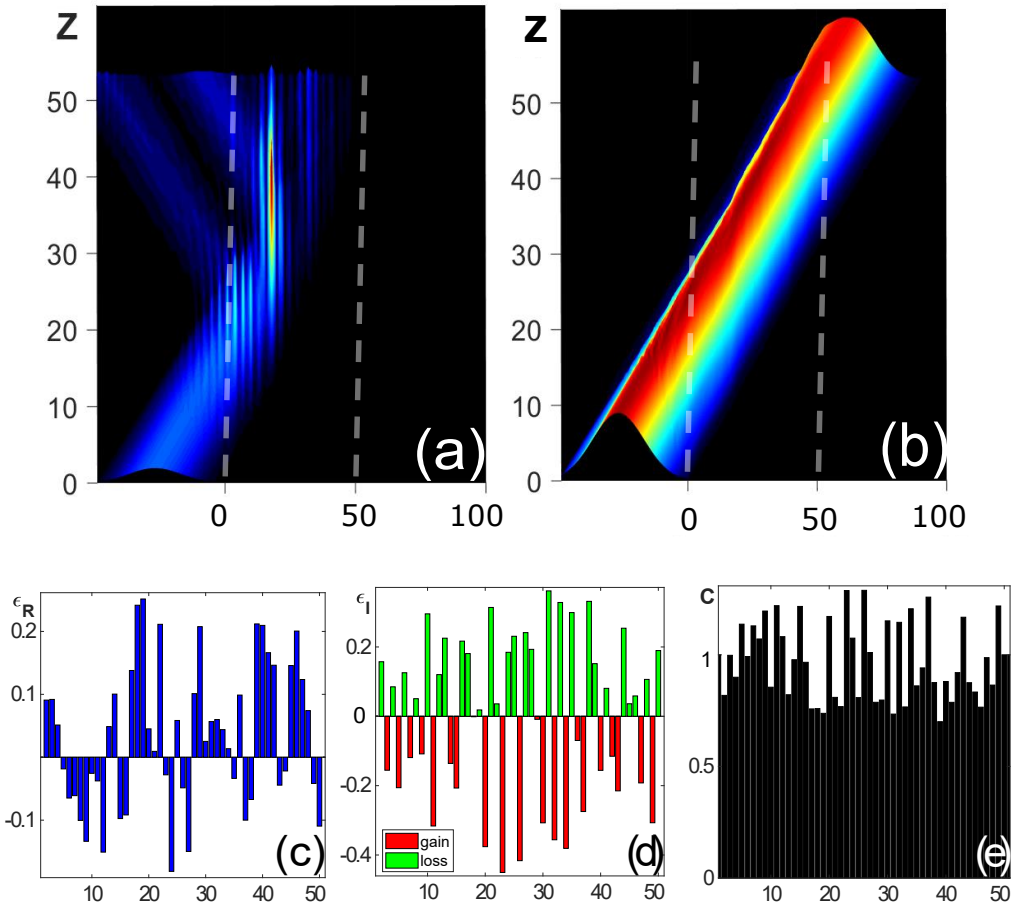

Figure 5.4: (a) Intensity of a beam propagating in a lattice with random real couplings. (b) Same as in (a) but with the potential of the form of Eq. 5.15 which supports constant intensity solutions. Dashed lines denote the interfaces among the sublattices. Real (c) and imaginary (d) part of the potential and coupling distribution (e) for the results shown above. In all the figures above the x-axis represents the waveguide number j. For these graphs we have set: $M = 50$, $j_0 = -37.5$ and $\sigma = 30$.

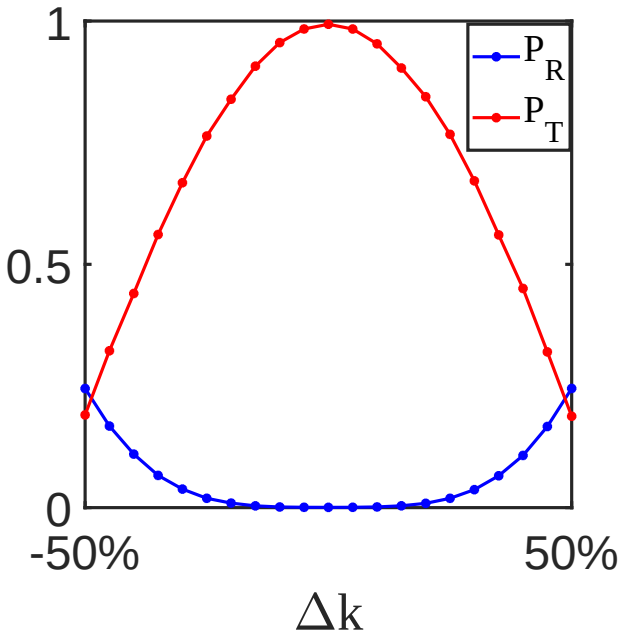

Figure 5.5: Power of the transmitted ($\mathcal{P}_T$, red line) and reflected ($\mathcal{P}_R$, blue line) wave, divided by the power of the initial beam (Eq. 5.14), as a function of the percentage deviation (detuning) from the required wavelength value k_x: $\Delta k = k'_x - k_x$. In this case we have set $k_x = \frac{\pi}{2}$, for the case of off-diagonal disorder. An averaging over 500 realizations of disorder has been performed for these results.

Conclusions

In conclusion, this thesis provides a systematic study of the localization phenomena in non-Hermitian disordered photonic lattices.

In Ch. 3 we examined the localization properties of the eigenmodes of 2-D optical lattices, in the presence of uniform non-Hermitian disorder. We have found that the spectrum of such a system forms an approximate ellipse on the complex plane, with the eigenvalues located near the middle of the ellipse to correspond to the less localized eigenfunctions. In addition, the breaking of time reversal symmetry in the non-Hermitian case, favors delocalization for weak disorder, while, as disorder is increased, the localization induced by the non-Hermitian disorder appears to be even stronger than in the Hermitian case. Finally, the level spacing distribution seems to obey a sub-Wigner probability distribution, when non-Hermitian disorder of intermediate amplitude is applied.

In Ch. 4 we studied the spectral and wave dynamic characteristics of non-Hermitian 1-D lattices with binary pair-correlated disorder. We found that the short range correlation of the randomness parameter leads to unexpected spectral features: for intermediate degree of randomness, appears to have a fractal-like intricate structure, and for higher values of the imaginary randomness parameter many eigenvalues are concentrated in very small areas of the complex plane. Even more surprising is what appears to be a general feature namely, in spite of the fact that all eigenfunctions are localized, transport by spatial jumps seems to be possible due to the partial overlap of the excited eigenmodes. We also found that our theoretical/numerical predictions are in good agreement with recent experimental findings.

Finally, in Ch. 5, we presented a systematic methodology to eliminate reflection due to disorder in realistic discrete systems consisting of coupled waveguides. In particular, we studied the perfect transmission of Gaussian wave packets through random, non-Hermitian optical lattices in $1 + 1$ dimensions. In the Hermitian limit, or even when the lattice has only loss or only gain elements, the transmission is low and the field is strongly distorted. However, for non-Hermitian disorder, where the real and the imagi-

nary parts are correlated in the way we describe, almost perfect transmission is achieved. Two different cases of on-diagonal (Wadati wave packets) and off-diagonal disorder are thoroughly examined and for both cases a near-perfect and shape-preserving transmission of an incoming Gaussian wave packet is observed.

We believe that our systematic study will pave the way for the direct experimental realization of these new phenomena in integrated photonic waveguide structures. Also extensions of our findings to lasers and coherent perfect absorbers in disordered waveguide lattices should be within immediate reach.

Bibliography

[1] Felix Bloch. Uber die quantenmechanik der elektronen in kristallgittern. *Zeitschrift für physik*, 52(7-8):555–600, 1929.

[2] Felix Bloch. *The Beginnings of Solid State Physics. A symposium organized by Nevill Mott*, volume 371. The Royal Society of London, series A, 1971.

[3] Philip W Anderson. Absence of diffusion in certain random lattices. *Physical review*, 109(5):1492, 1958.

[4] Elihu Abrahams, PW Anderson, DC Licciardello, and TV Ramakrishnan. Scaling theory of localization: Absence of quantum diffusion in two dimensions. *Physical Review Letters*, 42(10):673, 1979.

[5] Aart Lagendijk, Bart Van Tiggelen, and Diederik S Wiersma. Fifty years of anderson localization. *Phys. Today*, 62(8):24–29, 2009.

[6] Tsuneya Ando, Alan B Fowler, and Frank Stern. Electronic properties of two-dimensional systems. *Reviews of Modern Physics*, 54(2):437, 1982.

[7] Patrick A Lee and Daniel S Fisher. Anderson localization in two dimensions. *Physical Review Letters*, 47(12):882, 1981.

[8] Tomi Ohtsuki, Keith Slevin, and Tohru Kawarabayashi. Review of recent progress on numerical studies of the anderson transition. *Annalen der Physik*, 8(7-9):655–664, 1999.

[9] AD Zdetsis, CM Soukoulis, EN Economou, and Gary S Grest. Localization in two-and three-dimensional systems away from the band center. *Physical Review B*, 32(12):7811, 1985.

[10] JB Pendry. The evolution of waves in disordered media. *Journal of Physics C: Solid State Physics*, 15(16):3493, 1982.

[11] Nevill Francis Mott and Edward A Davis. *Electronic processes in non-crystalline materials*. Oxford university press, 2012.

[12] Ilia Mikhauilovich Lifshitz, Sergei Andreevich Gredeskul, and Leonid Andreevich Pastur. *Introduction to the theory of disordered systems*. Wiley-Interscience, 1988.

[13] Yoseph Imry. *Introduction to mesoscopic physics*. Number 2. Oxford University Press on Demand, 2002.

[14] Eleftherios N Economou. *Green's functions in quantum physics*, volume 3. Springer, 1983.

[15] Philos Landauer. Mag. 21, 863 (1970); m. büttiker. *Phys. Rev. Lett*, 57:1761, 1986.

[16] EN Economou and CM Soukoulis. Static conductance and scaling theory of localization in one dimension. *Physical Review Letters*, 46(9):618, 1981.

[17] Supriyo Datta. *Electronic transport in mesoscopic systems*. Cambridge university press, 1997.

[18] Bernhard Kramer and Angus MacKinnon. Localization: theory and experiment. *Reports on Progress in Physics*, 56(12):1469, 1993.

[19] EG Van Putten, D Akbulut, J Bertolotti, Willem L Vos, Aart Lagendijk, and AP Mosk. Scattering lens resolves sub-100 nm structures with visible light. *Physical review letters*, 106(19):193905, 2011.

[20] Ori Katz, Eran Small, Yaron Bromberg, and Yaron Silberberg. Focusing and compression of ultrashort pulses through scattering media. *Nature photonics*, 5(6):372, 2011.

[21] Nicolas Bachelard, Sylvain Gigan, Xavier Noblin, and Patrick Sebbah. Adaptive pumping for spectral control of random lasers. *Nature physics*, 10(6):426, 2014.

[22] Thomas Hisch, Matthias Liertzer, Dionyz Pogany, Florian Mintert, and Stefan Rotter. Pump-controlled directional light emission from random lasers. *Physical review letters*, 111(2):023902, 2013.

[23] Stefan Rotter and Sylvain Gigan. Light fields in complex media: Mesoscopic scattering meets wave control. *Reviews of Modern Physics*, 89(1):015005, 2017.

[24] Tal Schwartz, Guy Bartal, Shmuel Fishman, and Mordechai Segev. Transport and anderson localization in disordered two-dimensional photonic lattices. *Nature*, 446(7131):52, 2007.

[25] Yoav Lahini, Assaf Avidan, Francesca Pozzi, Marc Sorel, Roberto Morandotti, Demetrios N Christodoulides, and Yaron Silberberg. Anderson localization and nonlinearity in one-dimensional disordered photonic lattices. *Physical Review Letters*, 100(1):013906, 2008.

[26] Arash Mafi. Transverse anderson localization of light: a tutorial. *Advances in Optics and Photonics*, 7(3):459–515, 2015.

[27] CM Soukoulis, S Datta, and EN Economou. Propagation of classical waves in random media. *Physical Review B*, 49(6):3800, 1994.

[28] Peter Markos and Costas M Soukoulis. *Wave propagation: from electrons to photonic crystals*
and left-handed materials. Princeton University Press, 2008.

[29] Sajeev John. Strong localization of photons in certain disordered dielectric superlattices. *Physical review letters*, 58(23):2486, 1987.

[30] Eli Yablonovitch. Inhibited spontaneous emission in solid-state physics and electronics. *Physical review letters*, 58(20):2059, 1987.

[31] Eli Yablonovitch and TJ Gmitter. Photonic band structure: the face-centered-cubic case. *Physical Review Letters*, 63(18):1950, 1989.

[32] KM Ho, Che Ting Chan, and Costas M Soukoulis. Existence of a photonic gap in periodic dielectric structures. *Physical Review Letters*, 65(25):3152, 1990.

[33] Eli Yablonovitch, TJ Gmitter, and Kok-Ming Leung. Photonic band structure: The face-centered-cubic case employing nonspherical atoms. *Physical review letters*, 67(17):2295, 1991.

[34] Kin Ming Ho, CT Chan, CM Soukoulis, R Biswas, and M Sigalas. Photonic band gaps in three dimensions: new layer-by-layer periodic structures. *Solid State Communications*, 89(5):413–416, 1994.

[35] John D Joannopoulos, Pierre R Villeneuve, and Shanhui Fan. Photonic crystals. *Solid State Communications*, 102(2-3):165–173, 1997.

[36] Costas M Soukoulis. *Photonic crystals and light localization in the 21st century*, volume 563. Springer Science & Business Media, 2012.

[37] Michael M Sigalas and Eleftherios N Economou. Elastic and acoustic wave band structure. *Journal of Sound Vibration*, 158:377–382, 1992.

[38] Mihail Sigalas, Manvir S Kushwaha, Eleftherios N Economou, Maria Kafesaki, Ioannis E Psarobas, and Walter Steurer. Classical vibrational modes in phononic lattices: theory and experiment. *Zeitschrift für Kristallographie-Crystalline Materials*, 220(9-10):765–809, 2005.

[39] Pierre A Deymier. *Acoustic metamaterials and phononic crystals*, volume 173. Springer Science & Business Media, 2013.

[40] Martin Maldovan. Sound and heat revolutions in phononics. *Nature*, 503(7475):209, 2013.

[41] Mahmoud I Hussein, Michael J Leamy, and Massimo Ruzzene. Dynamics of phononic materials and structures: Historical origins, recent progress, and future outlook. *Applied Mechanics Reviews*, 66(4):040802, 2014.

[42] Abdelkrim Khelif and Ali Adibi. *Phononic Crystals*. Springer, 2015.

[43] Guancong Ma and Ping Sheng. Acoustic metamaterials: From local resonances to broad horizons. *Science advances*, 2(2):e1501595, 2016.

[44] Allard P Mosk, Ad Lagendijk, Geoffroy Lerosey, and Mathias Fink. Controlling waves in space and time for imaging and focusing in complex media. *Nature photonics*, 6(5):283–292, 2012.

[45] Diederik S Wiersma. Disordered photonics. *Nature Photonics*, 7(3):188, 2013.

[46] Mordechai Segev, Yaron Silberberg, and Demetrios N Christodoulides. Anderson localization of light. *Nature Photonics*, 7(3):197, 2013.

[47] Stefan Rotter and Sylvain Gigan. Light fields in complex media: Mesoscopic scattering meets wave control. *Reviews of Modern Physics*, 89(1):015005, 2017.

[48] Ivo M Vellekoop, Aart Lagendijk, and AP Mosk. Exploiting disorder for perfect focusing. *Nature photonics*, 4(5):320–322, 2010.

[49] Benoît Gérardin, Jérôme Laurent, Arnaud Derode, Claire Prada, and Alexandre Aubry. Full transmission and reflection of waves propagating through a maze of disorder. *Physical review letters*, 113(17):173901, 2014.

[50] Chia Wei Hsu, Seng Fatt Liew, Arthur Goetschy, Hui Cao, and A Douglas Stone. Correlation-enhanced control of wave focusing in disordered media. *Nature Physics*, 13(5):497–502, 2017.

[51] Ivo Micha Vellekoop and AP Mosk. Universal optimal transmission of light through disordered materials. *Physical review letters*, 101(12):120601, 2008.

[52] Abe Peña, A Girschik, F Libisch, S Rotter, and AA Chabanov. The single-channel regime of transport through random media. *Nature communications*, 5(1):1–8, 2014.

[53] Thomas Hisch, Matthias Liertzer, Dionyz Pogany, Florian Mintert, and Stefan Rotter. Pump-controlled directional light emission from random lasers. *Physical review letters*, 111(2):023902, 2013.

[54] Matthieu Davy and Azriel Z Genack. Selectively exciting quasi-normal modes in open disordered systems. *Nature communications*, 9(1):1–11, 2018.

[55] Vladimir V Konotop, Jianke Yang, and Dmitry A Zezyulin. Nonlinear waves in pt-symmetric systems. *Reviews of Modern Physics*, 88(3):035002, 2016.

[56] Liang Feng, Ramy El-Ganainy, and Li Ge. Non-hermitian photonics based on parity–time symmetry. *Nature Photonics*, 11(12):752–762, 2017.

[57] Greg Gbur and Konstantinos Makris. Introduction to non-hermitian photonics in complex media: Pt-symmetry and beyond. *Photonics Research*, 6(5):PTS1–PTS3, 2018.

[58] Ramy El-Ganainy, Konstantinos G Makris, Mercedeh Khajavikhan, Ziad H Musslimani, Stefan Rotter, and Demetrios N Christodoulides. Non-hermitian physics and pt symmetry. *Nature Physics*, 14(1):11–19, 2018.

[59] Stefano Longhi. Parity-time symmetry meets photonics: A new twist in non-hermitian optics. *EPL (Europhysics Letters)*, 120(6):64001, 2018.

[60] ŞK Özdemir, S Rotter, F Nori, and L Yang. Parity–time symmetry and exceptional points in photonics. *Nature materials*, 18(8):783–798, 2019.

[61] Mohammad-Ali Miri and Andrea Alù. Exceptional points in optics and photonics. *Science*, 363(6422):eaar7709, 2019.

[62] Carl M Bender and Stefan Boettcher. Real spectra in non-hermitian hamiltonians having p t symmetry. *Physical Review Letters*, 80(24):5243, 1998.

[63] Carl M Bender, Stefan Boettcher, and Peter N Meisinger. Pt-symmetric quantum mechanics. *Journal of Mathematical Physics*, 40(5):2201–2229, 1999.

[64] Carl M Bender, Dorje C Brody, and Hugh F Jones. Complex extension of quantum mechanics. *Physical Review Letters*, 89(27):270401, 2002.

[65] Nimrod Moiseyev. *Non-Hermitian quantum mechanics*. Cambridge University Press, 2011.

[66] Michael V Berry. Physics of nonhermitian degeneracies. *Czechoslovak journal of physics*, 54(10):1039–1047, 2004.

[67] WD Heiss. Exceptional points of non-hermitian operators. *Journal of Physics A: Mathematical and General*, 37(6):2455, 2004.

[68] M Liertzer, Li Ge, A Cerjan, AD Stone, Hakan E Türeci, and S Rotter. Pump-induced exceptional points in lasers. *Physical Review Letters*, 108(17):173901, 2012.

[69] Jan Wiersig, Sang Wook Kim, and Martina Hentschel. Asymmetric scattering and nonorthogonal mode patterns in optical microspirals. *Physical Review A*, 78(5):053809, 2008.

[70] Sang-Bum Lee, Juhee Yang, Songky Moon, Soo-Young Lee, Jeong-Bo Shim, Sang Wook Kim, Jai-Hyung Lee, and Kyungwon An. Observation of an exceptional point in a chaotic optical microcavity. *Physical review letters*, 103(13):134101, 2009.

[71] Konstantinos G Makris, R El-Ganainy, DN Christodoulides, and Ziad H Musslimani. Beam dynamics in p t symmetric optical lattices. *Physical Review Letters*, 100(10):103904, 2008.

[72] R El-Ganainy, KG Makris, DN Christodoulides, and Ziad H Musslimani. Theory of coupled optical pt-symmetric structures. *Optics letters*, 32(17):2632–2634, 2007.

[73] ZH Musslimani, Konstantinos G Makris, Ramy El-Ganainy, and Demetrios N Christodoulides. Optical solitons in p t periodic potentials. *Physical Review Letters*, 100(3):030402, 2008.

[74] A Guo, GJ Salamo, D Duchesne, R Morandotti, M Volatier-Ravat, V Aimez, GA Siviloglou, and DN Christodoulides. Observation of p t-symmetry breaking in complex optical potentials. *Physical Review Letters*, 103(9):093902, 2009.

[75] Christian E Rüter, Konstantinos G Makris, Ramy El-Ganainy, Demetrios N Christodoulides, Mordechai Segev, and Detlef Kip. Observation of parity–time symmetry in optics. *Nature physics*, 6(3):192–195, 2010.

[76] M Brandstetter, M Liertzer, C Deutsch, P Klang, J Schöberl, Hakan E Türeci, G Strasser, K Unterrainer, and S Rotter. Reversing the pump dependence of a laser at an exceptional point. *Nature communications*, 5(1):1–7, 2014.

[77] YD Chong, Li Ge, Hui Cao, and A Douglas Stone. Coherent perfect absorbers: time-reversed lasers. *Physical review letters*, 105(5):053901, 2010.

[78] Philipp Ambichl, Konstantinos G Makris, Li Ge, Yidong Chong, A Douglas Stone, and Stefan Rotter. Breaking of p t symmetry in bounded and unbounded scattering systems. *Physical Review X*, 3(4):041030, 2013.

[79] Liang Feng, Ye-Long Xu, William S Fegadolli, Ming-Hui Lu, José EB Oliveira, Vilson R Almeida, Yan-Feng Chen, and Axel Scherer. Experimental demonstration of a unidirectional reflectionless parity-time metamaterial at optical frequencies. *Nature materials*, 12(2):108–113, 2013.

[80] Hossein Hodaei, Mohammad-Ali Miri, Matthias Heinrich, Demetrios N Christodoulides, and Mercedeh Khajavikhan. Parity-time–symmetric microring lasers. *Science*, 346(6212):975–978, 2014.

[81] Sid Assawaworrarit, Xiaofang Yu, and Shanhui Fan. Robust wireless power transfer using a nonlinear parity–time-symmetric circuit. *Nature*, 546(7658):387–390, 2017.

[82] Zin Lin, Hamidreza Ramezani, Toni Eichelkraut, Tsampikos Kottos, Hui Cao, and Demetrios N Christodoulides. Unidirectional invisibility induced by p t-symmetric periodic structures. *Physical Review Letters*, 106(21):213901, 2011.

[83] Liang Feng, Ye-Long Xu, William S Fegadolli, Ming-Hui Lu, José EB Oliveira, Vilson R Almeida, Yan-Feng Chen, and Axel Scherer. Experimental demonstration of a unidirectional reflectionless parity-time metamaterial at optical frequencies. *Nature materials*, 12(2):108–113, 2013.

[84] Kevin Pichler, Matthias Kühmayer, Julian Böhm, Andre Brandstötter, Philipp Ambichl, Ulrich Kuhl, and Stefan Rotter. Random anti-lasing through coherent perfect absorption in a disordered medium. *Nature*, 567(7748):351–355, 2019.

[85] Joshua Feinberg and Anthony Zee. Non-hermitian random matrix theory: Method of hermitian reduction. *Nuclear Physics B*, 504(3):579–608, 1997.

[86] Stefano Longhi. Metal-insulator phase transition in a non-hermitian aubry-andré-harper model. *Physical Review B*, 100(12):125157, 2019.

[87] Diederik S Wiersma. The physics and applications of random lasers. *Nature physics*, 4(5):359–367, 2008.

[88] Sebastian Schönhuber, Martin Brandstetter, Thomas Hisch, Christoph Deutsch, Michael Krall, Hermann Detz, Aaron M Andrews, Gottfried Strasser, Stefan Rotter, and Karl Unterrainer. Random lasers for broadband directional emission. *Optica*, 3(10):1035–1038, 2016.

[89] David H Dunlap, HL Wu, and Philip W Phillips. Absence of localization in a random-dimer model. *Physical Review Letters*, 65(1):88, 1990.

[90] Konstantinos G Makris, Ziad H Musslimani, Demetrios N Christodoulides, and Stefan Rotter. Constant-intensity waves and their modulation instability in non-hermitian potentials. *Nature communications*, 6(1):1–7, 2015.

[91] Konstantinos G Makris, Ziad H Musslimani, Demetrios N Christodoulides, and Stefan Rotter. Constant intensity supermodes in non-hermitian lattices. *IEEE Journal of Selected Topics in Quantum Electronics*, 22(5):42–47, 2016.

[92] EMS Press. "Runge-Kutta method". Encyclopedia of Mathematics, 1994.

[93] Eleftherios N Economou. *The Physics of Solids: Essentials and Beyond*. Springer Science & Business Media, 2010.

[94] Jose M Escalante and Sergey E Skipetrov. Level spacing statistics for light in two-dimensional disordered photonic crystals. *Scientific reports*, 8(1):11569, 2018.

[95] FJ Dyson and ML Mehta. Random matrices and the statistical theory of energy levels iv. *J. math. Phys*, 4:701–12, 1963.

[96] Ryusuke Hamazaki, Kohei Kawabata, Naoto Kura, and Masahito Ueda. The threefold way in non-hermitian random matrices. *arXiv preprint arXiv:1904.13082*, 2019.

[97] G Marinello and MP Pato. Pseudo-hermitian ensemble of random gaussian matrices. *Physical Review E*, 94(1):012147, 2016.

[98] Yan V Fyodorov, Boris A Khoruzhenko, and Hans-Jürgen Sommers. Almost hermitian random matrices: crossover from wigner-dyson to ginibre eigenvalue statistics. *Physical review letters*, 79(4):557, 1997.

[99] Rainer Grobe, Fritz Haake, and Hans-Jürgen Sommers. Quantum distinction of regular and chaotic dissipative motion. *Physical review letters*, 61(17):1899, 1988.

[100] H Markum, R Pullirsch, and T Wettig. Non-hermitian random matrix theory and lattice qcd with chemical potential. *Physical review letters*, 83(3):484, 1999.

[101] Jean Ginibre. Statistical ensembles of complex, quaternion, and real matrices. *Journal of Mathematical Physics*, 6(3):440–449, 1965.

[102] Rainer Grobe and Fritz Haake. Universality of cubic-level repulsion for dissipative quantum chaos. *Physical review letters*, 62(25):2893, 1989.

[103] Yi Huang, BI Shklovskii, et al. Anderson transition in three-dimensional systems with non-hermitian disorder. *Physical Review B*, 101(1):014204, 2020.

[104] Vadim Oganesyan and David A. Huse. Localization of interacting fermions at high temperature. *Phys. Rev. B*, 75:155111, Apr 2007.

[105] Philip Phillips and Hong-Lu Wu. Localization and its absence: a new metallic state for conducting polymers. *Science*, 252(5014):1805–1812, 1991.

[106] V Bellani, E Diez, R Hey, L Toni, L Tarricone, GB Parravicini, F Domínguez-Adame, and R Gómez-Alcalá. Experimental evidence of delocalized states in random dimer superlattices. *Physical review letters*, 82(10):2159, 1999.

[107] U Naether, S Stützer, RA Vicencio, MI Molina, A Tünnermann, S Nolte, Tsampikos Kottos, DN Christodoulides, and A Szameit. Experimental observation of superdiffusive transport in random dimer lattices. *New Journal of Physics*, 15(1):013045, 2013.

[108] Philip George Harper. Single band motion of conduction electrons in a uniform magnetic field. *Proceedings of the Physical Society. Section A*, 68(10):874, 1955.

[109] Ariel Amir, Naomichi Hatano, and David R Nelson. Non-hermitian localization in biological networks. *Physical Review E*, 93(4):042310, 2016.

[110] Sebastian Weidemann, Mark Kremer, Stefano Longhi, and Alexander Szameit. Non-hermitian anderson transport. In *2020 Conference on Lasers and Electro-Optics (CLEO)*, pages 1–2. IEEE, 2020.

[111] II Yusipov, TV Laptyeva, and MV Ivanchenko. Quantum jumps on anderson attractors. *Physical Review B*, 97(2):020301, 2018.

[112] M Balasubrahmaniyam, Sandip Mondal, and Sushil Mujumdar. Necklace-state-mediated anomalous enhancement of transport in anderson-localized non-hermitian hybrid systems. *Physical Review Letters*, 124(12):123901, 2020.

[113] Konstantinos G Makris, Andre Brandstötter, Philipp Ambichl, Ziad H Musslimani, and Stefan Rotter. Wave propagation through disordered media without backscattering and intensity variations. *Light: Science & Applications*, 6(9):e17035, 2017.

[114] Andre Brandstötter, Konstantinos G Makris, and Stefan Rotter. Scattering-free pulse propagation through invisible non-hermitian media. *Physical Review B*, 99(11):115402, 2019.

[115] Sunkyu Yu, Xianji Piao, and Namkyoo Park. Bohmian photonics for independent control of the phase and amplitude of waves. *Physical review letters*, 120(19):193902, 2018.

[116] Etienne Rivet, Andre Brandstötter, Konstantinos G Makris, Hervé Lissek, Stefan Rotter, and Romain Fleury. Constant-pressure sound waves in non-hermitian disordered media. *Nature Physics*, 14(9):942–947, 2018.

[117] Vladimir V Konotop and Dmitry A Zezyulin. Families of stationary modes in complex potentials. *Optics letters*, 39(19):5535–5538, 2014.

[118] Miki Wadati. Construction of parity-time symmetric potential through the soliton theory. *Journal of the Physical Society of Japan*, 77(7):074005, 2008.

[119] SAR Horsley. Indifferent electromagnetic modes: Bound states and topology. *Physical Review A*, 100(5):053819, 2019.

[120] Vladimir V Konotop and Dmitry A Zezyulin. Construction of potentials with multiple spectral singularities. *arXiv preprint arXiv:2005.01383*, 2020.

[121] Enrique Outerelo et al. *Mapping degree theory*, volume 108. American Mathematical Soc., 2009.